




# Optimized design of an arterial network model reproduces characteristic central and peripheral haemodynamic waveform features of young adults

Avinash Kondiboyina<sup>1,2</sup> , Hilary A. Harrington<sup>1</sup>, Joseph J. Smolich<sup>1,2</sup> , Michael M. H. Cheung<sup>1,2,3</sup> and Jonathan P. Mynard<sup>1,2,4</sup> 

<sup>1</sup>Heart Research, Murdoch Children's Research Institute, Parkville, Victoria, Australia

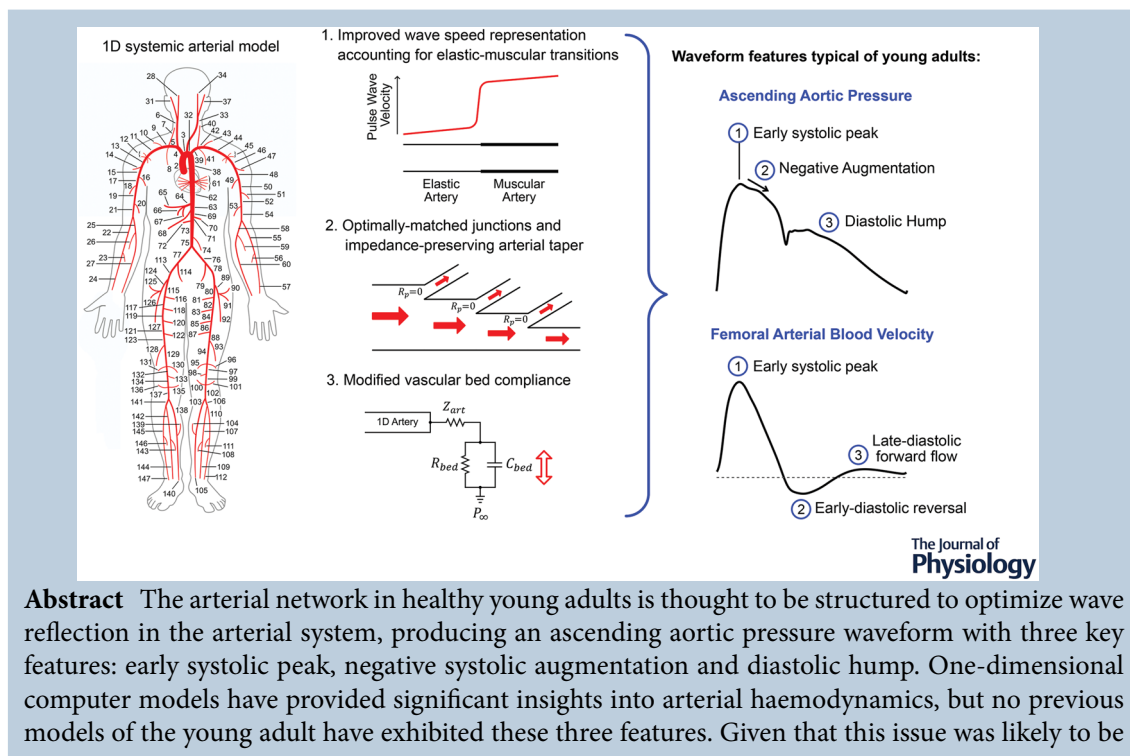
<sup>2</sup>Department of Paediatrics, University of Melbourne, Parkville, Victoria, Australia

<sup>3</sup>Department of Cardiology, Royal Children's Hospital, Parkville, Victoria, Australia

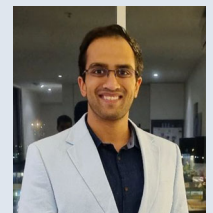
<sup>4</sup>Department of Biomedical Engineering, University of Melbourne, Parkville, Victoria, Australia

Handling Editors: Laura Bennet & Caroline Rickards

The peer review history is available in the Supporting information section of this article (<https://doi.org/10.1113/JP282942#support-information-section>).



**Avinash Kondiboyina** recently completed his PhD in biomedical engineering at Murdoch Children's Research Institute. He completed his Masters degree at Imperial College London and undergraduate studies at the University of Toronto. His current research is focused on using computational methods to investigate the effect of wave reflection on arterial haemodynamics. Using the model presented in this article, he will develop and validate new metrics to quantify the effect of wave reflection on the cardiovascular system. The goal of his research is to assess the potential utility of wave reflection to improve our understanding of cardiovascular disease mechanisms and risk quantification.



This article was first published as a preprint. Kondiboyina A, Harrington HA, Smolich JJ, Cheung MMH, Mynard JP. 2022. Optimised design of an arterial network model reproduces characteristic central and peripheral hemodynamic waveform features in young adults. Preprints. <https://doi.org/10.20944/preprints202203.0230.v1>.

related to unrepresentative or non-optimized impedance properties of the model arterial networks, we developed a new 'YoungAdult' model that incorporated the following features: (i) a new and more accurate empirical equation for approximating wave speeds, based on area and relative distance to elastic–muscular arterial transition points; (ii) optimally matched arterial junctions; and (iii) an improved arterial network geometry that eliminated 'within-segment' taper (which causes wave reflection in conduit arteries) whilst establishing 'impedance-preserving' taper. These properties of the model led to wave reflection occurring predominantly at distal vascular beds, rather than in conduit arteries. The model predicted all three typical characteristics of an ascending aortic pressure waveform observed in young adults. When compared with non-invasively acquired pressure and velocity measurements (obtained via tonometry and Doppler ultrasound in seven young adults), the model was also shown to reproduce the typical waveform morphology observed in the radial, brachial, carotid, temporal, femoral and tibial arteries. The YoungAdult model provides support for the concept that the arterial tree impedance in healthy young adults is exquisitely optimized, and it provides an important baseline model for investigating cardiovascular changes in ageing and disease states.

(Received 6 February 2022; accepted after revision 8 July 2022; first published online 19 July 2022)

**Corresponding author** Jonathan P. Mynard: Heart Research, Murdoch Children's Research Institute, 50 Flemington Road, Parkville, VIC 3052, Australia. Email: jonathan.mynard@mcri.edu.au

**Abstract figure legend** In this paper, three key improvements were implemented in a one-dimensional (1D) model of the systemic arterial network. (1) Wave speed was represented better by accounting for differences between elastic and muscular arteries via transition points. (2) Continuous arterial taper was replaced with stepwise reduction in diameter via well-matched side-branches. (3) Vascular bed compliance was modified to achieve triphasic flow in peripheral arteries. These improvements produced an ascending aortic pressure waveform with three features typical of a healthy young adult: an early systolic peak, negative augmentation and a diastolic hump.

### Key points

- The origin of wave reflection in the arterial system is controversial, but reflection properties are likely to give rise to characteristic haemodynamic features in healthy young adults, including an early systolic peak, negative systolic augmentation and diastolic hump in the ascending aortic pressure waveform, and triphasic velocity profiles in peripheral arteries. Although computational modelling provides insights into arterial haemodynamics, no previous models have predicted all these features.
- An established arterial network model was optimized by incorporating the following features: (i) a more accurate representation of arterial wave speeds; (ii) precisely matched junctions; and (iii) impedance-preserving tapering, thereby minimizing wave reflection in conduit arteries in the forward direction. Comparison with *in vivo* data ( $n = 7$  subjects) indicated that the characteristic waveform features in young adults were predicted accurately.
- Our findings strongly imply that a healthy young arterial system is structured to optimize wave reflection in the main conduit arteries and that reflection of forward waves occurs primarily in the vicinity of vascular beds.

### Introduction

It is widely recognized that a healthy arterial system limits the rise in pressure during systole and maintains pressure during diastole (Nichols, 1998; O'Rourke, 1982). One prominent view is that this occurs, in part, owing to the 'beautifully designed ... tuning' of the arterial tree (O'Rourke & Hashimoto, 2007), with junctions that are well matched in the forward direction (Papageorgiou

et al., 1990) resulting in reflected pressure waves predominantly arriving at the left ventricle during diastole. In the ascending aorta, this is evidenced by a type C waveform, which has a similar shape to the flow waveform during systole (with an early systolic peak and negative augmentation index; Kelly et al., 1989) and a pressure 'hump' during diastole that supports coronary perfusion (Murgo et al., 1980; Nichols et al., 1985; O'Rourke & Hashimoto, 2007). According to this model, arterial

stiffening with ageing causes wave reflections to arrive during systole, which contributes to systolic hypertension, elevated left ventricular afterload and, ultimately, cardiovascular events and mortality (Chirinos et al., 2012a, 2012b; Lee & Oh, 2010; Sluyter et al., 2019; Tomiyama et al., 2018; Zhou et al., 2021).

One-dimensional (1D) mathematical modelling of the arterial network is a powerful approach for gaining insight into the structural and functional properties that lead to this 'beautiful tuning', in addition to mechanisms underlying the detrimental effects of vascular ageing and disease (Alastruey et al., 2009; Charlton et al., 2019; Stergiopoulos et al., 1992). It therefore stands to reason that establishing a representative model of a healthy young adult is a crucial starting point for studying processes that might cause a departure from an 'ideal' arterial design. In particular, an accurate model of a young adult would be expected to exhibit the following characteristic features in the ascending aorta: (i) an early systolic peak; (ii) a negative augmentation; and (iii) a prominent diastolic hump. However, although the detailed model of Blanco et al. (2014) produced a diastolic hump, to our knowledge no previous models have predicted an early systolic peak and negative augmentation (Charlton et al., 2019; Mynard & Smolich, 2015; Reymond et al., 2012).

The reason(s) why these features have not been captured well in existing 1D models is unclear, given that input variables, such as wave speed in the ascending aorta (Groenink et al., 1998; Kim et al., 2013; Negoita et al., 2018; Rogers et al., 2001), and general haemodynamic variables, such as systolic and diastolic blood pressures (Master et al., 1950; O'Rourke & Nichols, 2005; Robinson & Brucer, 1939) and cardiac output (Brandfonbrener et al., 1955; Katori, 1979), have been representative of young adults. Nonetheless, at least four possible reasons might be involved in current 1D models not capturing all key features of young adult blood pressure waveforms. The first reason is that the wave speeds for the other arteries might not have been sufficiently representative of *in vivo* values. Given that it is not feasible to obtain *in vivo* data from every artery in the body, previous investigators have estimated wave speeds of all arteries via an empirical equation that uses arterial diameter as the independent variable (Olufsen, 1999; Reymond et al., 2009). However, given that the common carotid and femoral arteries have comparable diameters [0.69 cm (Pomella et al., 2017) and 0.77 cm (Lorbeer et al., 2018), respectively], this approach leads to similar estimated wave speeds for both arteries. In contrast, *in vivo* measurements indicate that wave speed in the carotid artery [397–485 cm s<sup>-1</sup> (Engelen et al., 2015; Jourdan et al., 2005; Mikola et al., 2015; Petersen et al., 2006; Rakobowchuk et al., 2008)] is substantially lower than in the femoral artery [926–1029 cm s<sup>-1</sup> (Bossuyt et al., 2015; De Hoon et al., 2003; Rakobowchuk et al., 2009; van den Berkortel et al., 1998)], most likely

because the common carotid is an 'elastic artery' (i.e. has a higher elastin content), whereas the femoral artery is a 'muscular artery' (higher smooth muscle content) (Learoyd & Taylor, 1966; Leloup et al., 2015; Lockwood et al., 1992). As a rule of thumb, systemic arteries that are closer to the heart (e.g. aorta and carotid) are elastic, whereas those further away (femoral and radial) are muscular (Betts et al., 2013: 892–893). In this paper, we propose a new method for estimating the wave speed of all systemic arteries that accounts for the relative distance to transition points from elastic to muscular arteries.

A second possibility for the lack of young adult features in previous models is non-representative wave reflection properties of the arterial tree, given the profound influence of wave reflection on haemodynamic waveforms (van den Bos et al., 1982). As previous models have exhibited positive systolic augmentation (Blanco et al., 2014; Charlton et al., 2019; Mynard & Smolich, 2015; Reymond et al., 2012), wave reflection in these models is likely to have occurred more proximally than is typical in young adults owing to certain features of these geometrically simplified models. For example, similar to the related models by other authors (Avolio, 1980; Blanco et al., 2014; Reymond et al., 2009; Sherwin et al., 2003; Stergiopoulos et al., 1992; Westerhof et al., 1969), the model by Mynard and Smolich (2015) incorporated a substantial amount of taper in the brachial and femoral arteries (70 and 50% reduction in area, respectively) and no side-branches along their substantial length (35 and 44 cm, respectively). Such taper in the models is likely to produce substantial wave reflection (Segers & Verdonck, 2000). Although the exact origin of wave reflection in the arterial system is controversial (Segers & Verdonck, 2000; Westerhof et al., 2008), one widely held theory is that wave reflection occurs mainly in the vicinity of resistance vessels (Hamilton, 1944; O'Rourke, 1984). If this is the case, it is likely that the progressive decline in diameter of conduit arteries with distance from the heart occurs primarily in a stepwise manner (decreasing where side-branches arise), which allows for the preservation of impedance and minimizes wave reflection of forward waves in the main conduit arteries. This stepwise reduction in diameter might therefore be considered 'impedance-preserving taper', in contradistinction to 'within-segment taper' that increases impedance and gives rise to wave reflection.

A third issue concerns the degree of wave reflection occurring at the distal vascular beds. In many previous models, the simulated velocity waveforms in peripheral arteries (such as the femoral artery) have been monophasic (forward flow throughout the cardiac cycle; Reymond et al., 2009; Stergiopoulos et al., 1992), whereas *in vivo* waveforms are triphasic (forward flow during systole, reverse flow during early diastole, and forward flow again during late diastole; Hwang, 2017; Kim et al., 2020). It has been suggested that the early diastolic reverse

flow arises owing to the high resistance of peripheral vascular beds (Maixner et al., 1980; Rittenhouse et al., 1976), which in turn is likely to be associated with lower vascular bed compliance. Importantly, vascular bed compliance (not resistance *per se*) governs the reactive (or pulsatile) components of impedance, hence the degree of wave reflection (Westerhof & Westerhof, 2018). However, although vascular bed compliance ( $C_{\text{bed}}$ ) is therefore likely to be a key parameter governing systemic arterial wave reflection, current methods of estimating  $C_{\text{bed}}$  for modelling studies are highly approximate. Thus, the *in vivo* value of  $C_{\text{bed}}$  is not known. In this paper, we therefore investigate the effect of  $C_{\text{bed}}$  on central and peripheral haemodynamics.

The fourth issue is that although most junctions in the systemic vasculature appear to be well matched in the forward direction (Papageorgiou et al., 1990), some studies suggest that the aorto-iliac bifurcation could be an exception to this rule, with a reflection coefficient ( $R_p$ ) as high as 0.2 in some individuals (Greenwald et al., 1990; Papageorgiou et al., 1990). However, the effect of wave reflection at the aorto-iliac bifurcation on the wave reflection patterns in the aorta has not been explored in previous models.

This study had three main aims. The first aim was to determine the effect of incorporating the following improved physiological variables on large artery pressure and flow waveforms into a 1D model previously described by Mynard and Smolich (2015): (i) a more accurate empirical equation that approximates arterial wave speeds based on cross-sectional area and relative distance to known elastic–muscular arterial transition points; and (ii) eliminating within-segment taper and ensuring that any taper in major arteries is impedance preserving (e.g. by adding additional side-branches). We hypothesized that this improved ‘YoungAdult’ model would predict early systolic peak, negative augmentation and diastolic hump in the ascending aortic pressure waveform, and triphasic velocity profiles in peripheral arteries. The second aim was to validate model predictions with non-invasively acquired *in vivo* pressure and velocity waveforms obtained from young adults, with a focus on whether the model reproduced key features of waveform morphology. The third aim was to determine the influence of the following key aspects of the model: (i) compliance of distal vascular beds; (ii) reflection coefficient of the aorto-iliac bifurcation; and (iii) use of impedance-preserving vs. within-segment arterial taper on arterial wave reflection.

## Methods

### Area-wave speed relationship

**Conventional approach.** Previous modelling studies defined the relationship between arterial diameter and

wave speed by fitting exponential (Olufsen, 1999) or power (Reymond et al., 2009) curves to *in vivo* data. In doing so, the elastic/muscular nature of arteries has not been accounted for explicitly. To evaluate this approach, *in vivo* data on the wave speeds of various arteries in young adults (18–30 years of age) were gathered from the literature, the details of which are presented in Appendix A. Similar to previous work, a power relationship [eqn (1)] was fitted to the wave speed and area data points using the Curve Fitting toolbox of MATLAB (MathWorks, Natick, MA, USA). Furthermore, an anchor point was imposed for the fitted curve at the wave speed of the ascending aorta (segment 2), because we considered this to be the most important value for achieving representative arterial compliance. To achieve this, a weight of one was given to the wave speeds of all other arteries, while the weight of the ascending aortic wave speed was increased arbitrarily to a value (50) that forced the curve to pass exactly through this wave speed. This manipulation did not significantly alter the shape of the curve in comparison to using no weights (data not shown). The resulting power law equation was as follows:

$$c = \frac{577.3}{A^{0.23}}, \quad (1)$$

where  $c$  is the wave speed (in centimetres per second) and  $A$  is the area of the artery (in centimetres squared). This relationship yielded an  $R^2$  value of 0.79 and a root mean square error (RMSE) of  $177 \text{ cm s}^{-1}$  (Fig. 1A). However, there were substantial differences between the *in vivo* wave speeds and those calculated using this equation (Fig. 1B). For example, the *in vivo* wave speeds of the carotid and femoral arteries were  $438$  and  $905 \text{ cm s}^{-1}$  (average of literature values; refer to Appendix A), respectively, whereas eqn (1) yielded  $679 \text{ cm s}^{-1}$  (difference =  $-241 \text{ cm s}^{-1}$ ) and  $703 \text{ cm s}^{-1}$  (difference =  $202 \text{ cm s}^{-1}$ ), respectively.

**Accounting for elastic–muscular transition points.** In addition to elastic arteries being closer to the heart and muscular arteries being further away, there are known transition points along a given arterial pathway where there is a substantial increase in wave speed and distinct change in morphological features from one artery to the next; this indicates a transition from predominantly elastic to more muscular arteries. These points are at the distal ends of the axillary artery for the upper limbs (Bjarnegård & Länne, 2010) and the abdominal aorta for the lower limbs (Latham et al., 1985), and 1 cm from the origin of the external carotid artery for the head and neck region (Nowrozani & Zareian, 2011) [we here assume the same distance for the internal carotid artery, consistent with its classification as a muscular artery (Rees, 1968)]. Using this, we propose a ‘transition distance index’ (TDI) of an artery as a surrogate marker for its

degree of elasticity/muscularity. The TDI is defined as the distance between the proximal end of an artery and the left ventricle divided by the distance between the transition point and the left ventricle. Thus,  $TDI < 1$  indicates an elastic artery and  $TDI > 1$  a muscular artery.

The transition points at the axillary artery, abdominal aorta and external carotid artery were assigned to the arm arteries (subclavian to ulnar and radial arteries), the entire aorta and leg arteries (ascending aorta to posterior tibial artery) and the cerebral arteries (all arteries distal to the common carotid and vertebral arteries inclusive), respectively. The TDIs of arteries with available *in vivo* data on wave speed and area are shown in Appendix A. Power and sigmoid functions were used to govern the area dependence and TDI dependence of wave speed, respectively. Thus, a three-dimensional surface was

obtained, with area and TDI as independent variables and wave speed as the dependent variable [eqn (2)]. After weighting towards the ascending aortic data point in the same way as for eqn (1), the final expression was as follows:

$$c = \frac{661}{A^{0.058}} + 145.3 \times \arctan(167 \times TDI - 164.8). \quad (2)$$

This relationship yielded an  $R^2$  value of 0.98 and RMSE of  $57 \text{ cm s}^{-1}$  (Fig. 1C). The differences between the *in vivo* wave speeds and those calculated using the new relationship were substantially reduced in comparison to those obtained with eqn (1) (Fig. 1D), with values of 462 and  $921 \text{ cm s}^{-1}$  for the carotid and femoral arteries, respectively (differences of only  $-24$  and  $-15 \text{ cm s}^{-1}$  from the *in vivo* values, respectively; see Appendix A).

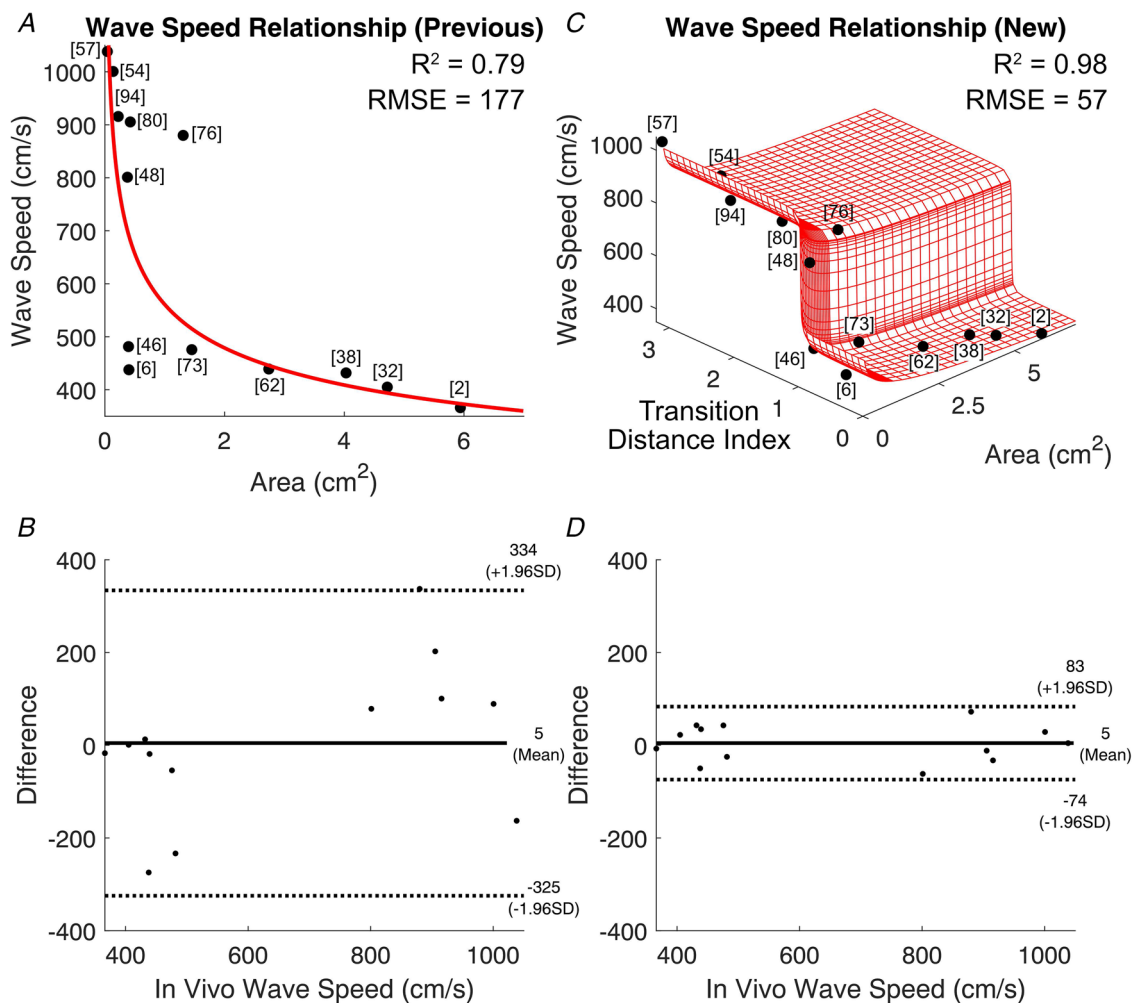


**Figure 1. Area-wave speed relationship**  
 A and C, wave speed estimated only from arterial area as in previous studies (A) and that estimated from the arterial area and transition distance index in the present study (C). The numbers in square brackets indicate the segment number of the artery (see Fig. 2). B and D, Bland–Altman plots depicting the difference between *in vivo* wave speeds and those calculated using the previous and new relationships, respectively. Abbreviation: RMSE, root mean square error. [Colour figure can be viewed at [wileyonlinelibrary.com](http://wileyonlinelibrary.com)]

## Model development

The 1D YoungAdult model described herein is an adaptation of a previously developed closed-loop model of the entire circulation and four-chamber heart, herein referred to as 'Mynard2015' (Mynard & Smolich, 2015). Given that the present study relates to only systemic arterial haemodynamics, only those model components likely to have a substantial impact on large artery haemodynamics were incorporated; therefore, the coronary arteries, veins and the pulmonary circulation were removed, whereas the cerebral arteries were retained, because these have been shown to have an effect on central waveforms (Reymond et al., 2009). The input to the YoungAdult model was a two-chamber elastance-based heart model (left atrium and ventricle) that has been described previously (Kondiboyina et al., 2020). The distal arteries were terminated with lumped-parameter three-element Windkessel compartments representing downstream vascular beds.

Elimination of the veins, pulmonary and coronary circulations and interventricular interactions caused small changes in the preload, mean arterial pressure and chamber elastance, respectively, compared with the closed-loop model. To achieve results that were similar to those of the Mynard2015 model, we used an algorithm to adjust the preload, vascular resistance and chamber elastance iteratively until the maximal chamber volume, mean aortic pressure and maximum effective chamber elastance, respectively, of the YoungAdult model were within a 0.5% tolerance of those of the Mynard2015 model. Further details about the model are provided in Appendix B.

**Tapering and arterial side-branches.** To obtain impedance-preserving taper and reduce early wave reflection, side-branches were added to the major arterial segments of the YoungAdult model, such as the internal carotid, radial, brachial and femoral arteries. The brachial artery, which originally had a 71% area taper, was divided into four non-tapered segments of successively smaller diameters by adding side-branches along its length based on the detailed model of Blanco et al. (2014). Likewise, the femoral artery, which originally had an area taper of 43%, was divided into five non-tapered segments of successively smaller diameters by adding four equally spaced side-branches representing the muscular branches of the femoral artery that perfuse the surrounding tissue. Furthermore, a more detailed lower limb arterial network was included in the model by including the genicular, popliteal and peroneal arteries, which have been neglected in most previous models. Figure 2 depicts a schematic representation of the model, and the details of all arteries included in the YoungAdult model can be found in Supplemental File 1.

**Impedance matching of branch junctions.** Arterial junctions have been found to be relatively well matched *in vivo* (i.e.  $R_p$  of approximately zero), implying an efficient transmission of energy in the forward direction (Papageorgiou et al., 1990). However, simply eliminating within-segment taper from arteries of the YoungAdult model would result in unmatched junctions. We therefore developed an optimization algorithm to produce well-matched junctions along the arterial tree of the YoungAdult model. The  $R_p$  value at a junction can be calculated using eqn (3), as follows:

$$R_p = \frac{(A_0/c_0) - (A_1/c_1) - (A_2/c_2)}{(A_0/c_0) + (A_1/c_1) + (A_2/c_2)}, \quad (3)$$

where the subscript '0' refers to the parent artery, while '1' and '2' refer to the two daughter arteries. As part of the optimization algorithm, the area and wave speed of the parent artery were kept fixed, while  $A_1$  and  $A_2$  were multiplied by an unknown factor ( $x$ ); the corresponding wave speeds ( $c_1$  and  $c_2$ ) were calculated using eqn (2). Using the `fminsearch` function of MATLAB, the value of  $x$  was changed iteratively until a reflection coefficient of zero was achieved (within a tolerance of  $\pm 0.001$ ). In this manner, the optimization was highly constrained by altering only the areas; there were some downstream effects on wave speed and wall visco-elastic coefficient, which were determined by the arterial area [eqn (2)] and diameter [eqn (B5); Appendix B], respectively. Furthermore, the optimization algorithm did not significantly alter the diameters of the downstream arteries, as evidenced by the terminal posterior tibial (Black et al., 2003; Sabatier et al., 2006) and radial arteries (Beniwal et al., 2014; Yoo et al., 2003, 2005), which had diameters within physiological ranges. Note that the within-segment taper of the cerebral arteries downstream of the internal carotid artery from the Mynard2015 model was retained because the looping nature of the cerebral arterial tree meant that some cerebral arteries had two parents. This is not conducive for the optimization algorithm, which requires a simple bifurcating tree structure.

To explore the influence of reflection at the aorto-iliac bifurcation, the optimization algorithm was used to obtain a second model, in which an  $R_p$  value of 0.2 was enforced at the aorto-iliac bifurcation, along with well-matched junctions in the downstream junctions of the legs.

**Vascular bed compliance.** The vascular beds were represented by Windkessel models (Appendix B). The compliance of distal vascular beds ( $C_{bed}$ ) is difficult to measure *in vivo*, and estimation techniques are therefore used for model parameterization. In most studies, total arterial compliance ( $TAC_{wk}$ ) has first been estimated from aortic pressure and flow waveforms via the pulse pressure

method that uses a two-element Windkessel model (Stergiopoulos et al., 1994). Vascular bed compliance is then estimated by subtracting the combined compliance of all 1D arterial segments from  $TAC_{wk}$  and distributing the remaining compliance among the vascular beds (in inverse proportion to their resistances). Although the Windkessel method is well established to estimate arterial compliance, it is not known whether this ‘subtraction approach’ captures both central arterial compliance ( $C_{art}$ ) and  $C_{bed}$  accurately.

In Appendix C, we show that although  $TAC_{wk}$  is sensitive to  $C_{art}$ , it is relatively insensitive to  $C_{bed}$  in the YoungAdult model, with a 153% increase in total compliance of the model, produced by changing only  $C_{bed}$ ,

leading to an increase of only 1.6% in  $TAC_{wk}$ . This suggests that currently used methods of estimating  $C_{bed}$  might be inaccurate. We thus investigated the effect of varying  $C_{bed}$  on the model waveforms. The parameters  $C_{bed}$  and  $R_{bed}$  (Windkessel resistance) are related via an assumed time constant ( $\tau = R_{bed} \times C_{bed}$ ). Starting from a value of  $\tau = 0.55$ , as used in Mynard2015, we found that a value of  $\tau = 1.3$  produced the characteristic features of a young adult aortic pressure waveform (early systolic peak, diastolic hump and negative augmentation) and of the peripheral velocity waveforms (triphasic profile). Thus,  $C_{bed}$  of all vascular beds was calculated using  $R_{bed}$  and  $\tau = 1.3$  as the baseline model. The details of the vascular beds of the YoungAdult model with baseline values of  $C_{bed}$  can be

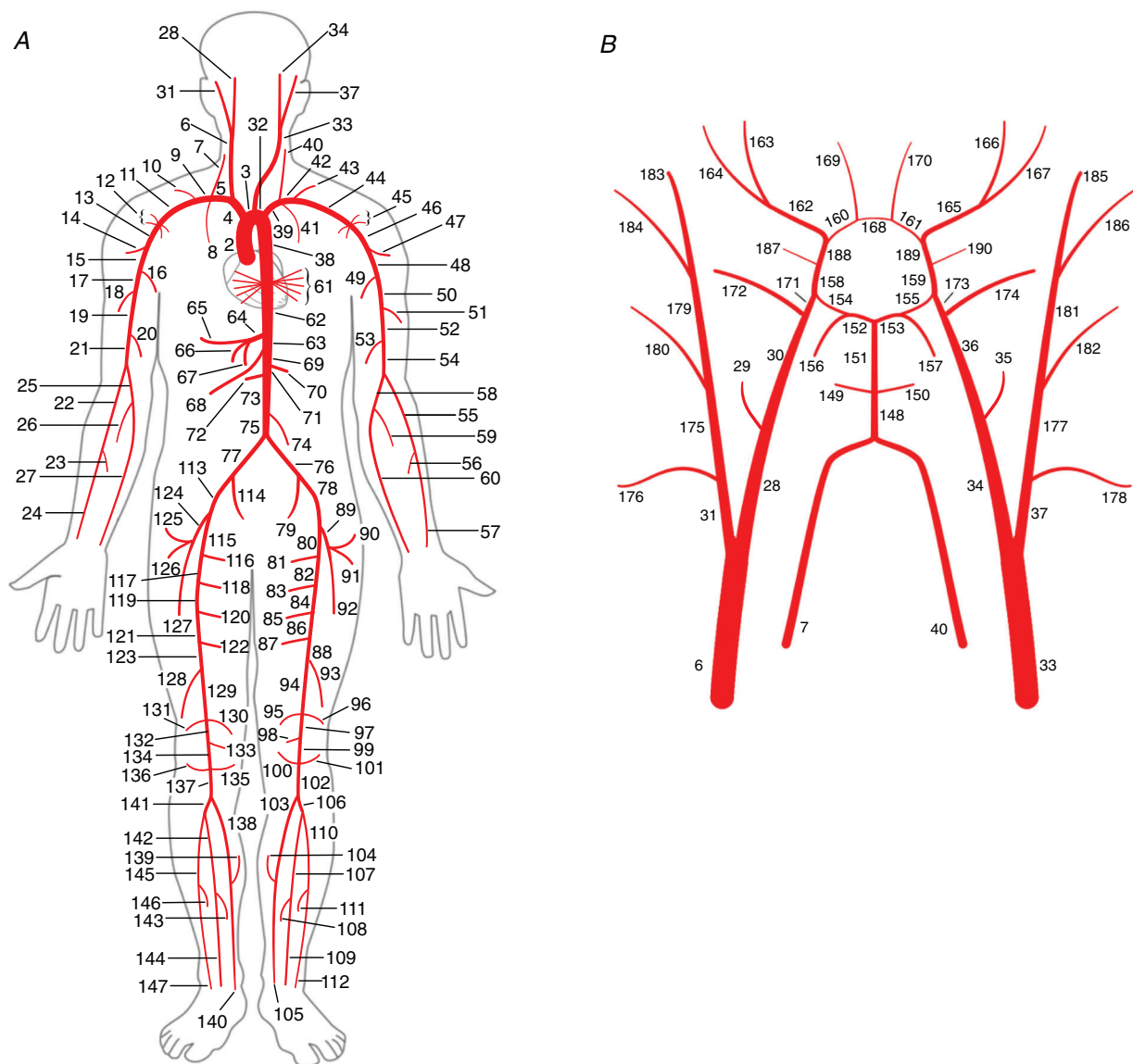


**Figure 2. Schematic diagram of the systemic (A) and cerebral (B) arteries of the YoungAdult model**  
 [Colour figure can be viewed at [wileyonlinelibrary.com](http://wileyonlinelibrary.com)]

found in Supplemental File 2. The sensitivity of the model to the value of  $\tau$  was also tested by performing simulations with  $\tau = 0.5$  and  $\tau = 2.5$ .

**Impact of impedance-preserving vs. within-segment taper.** To elucidate the impact of using impedance-preserving taper on central wave reflection, the closed-loop Mynard2015 model (with a substantial degree of within-segment taper) was first converted to an open-loop model, as described above, but without any other changes to the arterial tree geometry or wave speed. The  $C_{\text{bed}}$  of all vascular beds was then calculated based on  $R_{\text{bed}}$  and values of  $\tau$  of 1.3 (baseline) and 100 (used to reduce wave reflection markedly at vascular beds and thereby reveal the contribution of tapering to wave reflection). The same procedure was followed for the YoungAdult model, which has no within-segment taper (i.e. only impedance-preserving taper), except in the cerebral arteries. The waveforms at the aorta of the two models were then compared for both values of  $\tau$ .

To quantify the effects of taper on central wave reflection, we calculated the system 'input pressure' [ $P_{\text{in}}$ , elsewhere called the water hammer pressure (Vennin et al., 2021), which signifies the pressure that would occur in the absence of any wave reflection] as  $P_{\text{in}} = QZ_c$  (Phan et al., 2016), where  $Q$  is flow and  $Z_c$  is the characteristic impedance calculated using the frequency-domain method (O'Rourke & Taylor, 1967). Conversely, the 'total reflected pressure' ( $P_{\text{ref}}$ ), defined as the pressure arising from vascular wave reflection and any re-reflections occurring at the ventricle, is given by  $P_{\text{ref}} = P - P_{\text{in}} = 2P_{\text{bk}}$ , where  $P$  is the total pressure and  $P_{\text{bk}}$  is the traditionally defined backward component of pressure obtained by wave separation (Westerhof et al., 1972). In summary,  $P = P_{\text{in}} + P_{\text{ref}}$ , and as wave reflection decreases,  $P_{\text{ref}} \rightarrow 0$  and  $P \rightarrow P_{\text{in}}$  (Phan et al., 2016).

**Model computation.** The model was implemented using previously described methods (Mynard & Nithiarasu, 2008; Mynard & Smolich, 2015). In brief, the non-linear 1D form of the Navier–Stokes equations, combined with a non-linear viscoelastic pressure–area relationship (Mynard & Smolich, 2015), were solved using the locally conservative Galerkin finite element method (Mynard & Nithiarasu, 2008), with conservation of mass and continuity of total pressure enforced at junctions. For a detailed description, refer to Appendix B.

### Model validation with *in vivo* data

**Non-invasive study.** Model-predicted pressure and velocity waveforms were validated by performing applanation tonometry and Doppler ultrasound measurements, respectively, of accessible arteries in

seven healthy young adults aged between 21 and 25 years. Informed consent was obtained from all participants, and the study conformed to the standards set by the *Declaration of Helsinki*. The study was approved by the Ethics Committee of the Royal Children's Hospital, Victoria, Australia (HREC/74476/RCHM-2021). Participants were asked to refrain from consuming caffeine or alcohol for 3 h before the study, and all participants were non-smokers. They were placed in a supine position and were allowed to rest for 5 min before recording their brachial blood pressure with an oscillometric device (WatchBP Office Central; Microlife, Widnau, Switzerland). Pressure waveforms in the left brachial, radial, common carotid, superficial femoral, superficial temporal and posterior tibial arteries were then measured with applanation tonometry (SPT-301; Millar Instruments, Houston, TX, USA). The pressure waveform of the ascending aorta was obtained by applying a validated transfer function to the common carotid pressure waveform (Chen et al., 1996). Finally, Doppler ultrasonography was performed using a GE Vivid ultrasound machine (10–15 MHz; GE Healthcare, Parramatta, NSW, Australia) for the left common carotid and femoral arteries and a VisualSonics Vevo 3100 ultrasound machine (30–70 MHz; Fujifilm VisualSonics, Toronto, ON, Canada) for the left brachial, radial and posterior tibial arteries, owing to the difference in depth of the arteries. The sampling gate was over the middle two-thirds of the artery, with an insonation angle of  $<60^\circ$  (Gerhard-Herman et al., 2006). Doppler ultrasonography of the superficial temporal artery was not performed.

**Analysis of *in vivo* data.** Pressure waveforms from tonometry were averaged over  $\sim 20$  heart beats. Systolic and pulse pressures for each artery were obtained by calibrating the waveforms to diastolic and mean brachial pressures, because these pressures are similar throughout the arterial network (Hansen & Orskov, 1992; Kelly & Fitchett, 1992). The upper and lower spectral envelopes of the Doppler ultrasound data were automatically segmented using a custom program written in MATLAB 2019b (R2020b; The MathWorks, Natick, MA, USA). In each artery, the mean velocity waveform across three cycles was calculated from the spectrum-weighted average, from which an average velocity waveform was obtained.

To facilitate visual comparison of *in vivo* and model waveforms, the pressure and velocity waveforms were normalized to an amplitude of one. To normalize the systolic duration, pressure waveforms with a distinct diastolic notch (common carotid, superficial temporal and ascending aortic waveforms) were normalized to a systolic duration of 0.3 s (the same as that of the model). The waveforms in other arteries did not always



have a sharply defined dicrotic notch indicating the end of systole; therefore, these waveforms were scaled horizontally to minimize the root mean squared error compared with the corresponding model waveform. The pressure and velocity waveforms for each artery were then ensemble-averaged across all participants for visual validation of the corresponding waveforms produced by the model. Validation of raw absolute values of pressure and velocity (systolic and pulse) are also tabulated.

## Results

### Comparison with previous models

Figure 3 compares the aortic pressure waveforms from the YoungAdult model with those from previous models, which were extracted from published data. The YoungAdult model displayed all features typically found in young adults: early systolic peak (at 35% of systolic duration), negative augmentation (augmentation index =  $-3.6\%$ ) and a clear diastolic hump. In comparison, previous models exhibited later

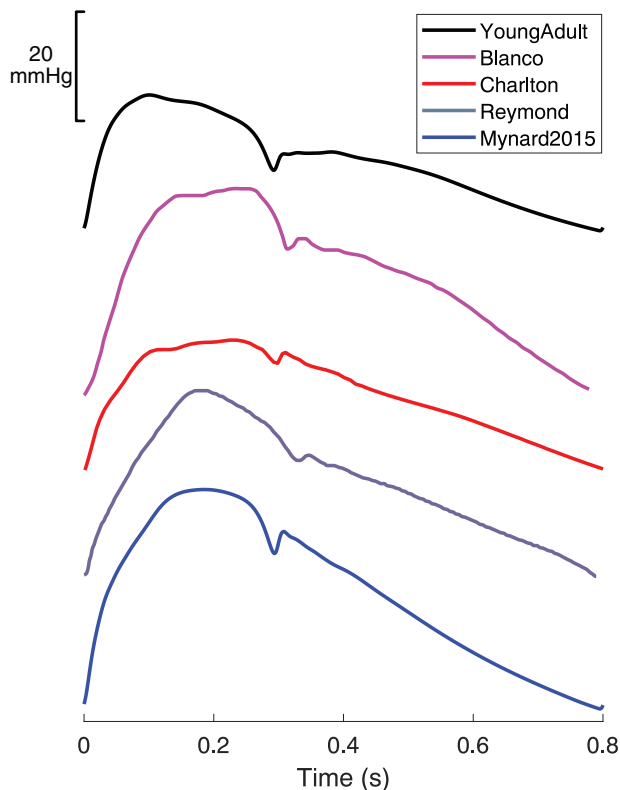


**Figure 3. Comparison of the YoungAdult model with models described in the literature**

Comparison of the ascending aortic pressure waveform of the YoungAdult model with models described by Blanco et al. (2014), Charlton et al. (2019), Reymond et al. (2012) and the Mynard2015 model (Mynard & Smolich, 2015). [Colour figure can be viewed at [wileyonlinelibrary.com](http://wileyonlinelibrary.com)]

**Table 1. Characteristics of participants in the *in vivo* validation study ( $n = 7$ )**

Characteristic	Value
Age (years)	22.6 $\pm$ 1.5*
Height (cm)	172.2 $\pm$ 7.8*
Weight (kg)	64.4 $\pm$ 15.7*
Sex (% male)	29

\*Data are presented as the mean  $\pm$  SD.

systolic peaks (between 53 and 75% of systolic duration) and positive augmentation (augmentation index between 3.4 and 24%), and only the Blanco model displayed a diastolic hump.

### *In vivo* validation

Participant characteristics are presented in Table 1, and the top panels of Figs 4–6 present the raw waveforms (pressure and velocity) of all seven participants in grey and the corresponding average waveforms in black; the raw data for the average waveforms are given in Supplemental File 3. There are no pressure scales in these figures because our primary aim was to visually compare the model waveforms with *in vivo* ones. Overall, pressure and velocity waveforms produced by the baseline YoungAdult model ( $\tau = 1.3$ ) were similar to those found *in vivo*. Importantly, the model captured key features of young adult waveforms, such as triphasic velocity profiles in distal arteries (brachial, radial, femoral and tibial) and an aortic pressure waveform that matched the *in vivo* waveform. Furthermore, Table 2 shows that the systolic and pulse pressures and the maximum and pulse velocity values of all arteries of the model were within the range of values found *in vivo*, with the exception of ascending aortic pulse pressure (although the model values were similar to the central pulse pressure reported in 18- to 29-year-olds in a much larger study (McEniery et al., 2005)).

### Influence of vascular bed compliance

Decreasing the compliance of the arm vascular beds by decreasing  $\tau$  increased the triphasic nature of the velocity waveforms of the brachial and radial arteries, with increasing amplitudes of the systolic forward velocity, early diastolic reverse velocity and late diastolic forward velocity, along with earlier diastolic velocity reversal. Similar changes were also observed in the pressure waveforms, with an increased systolic peak, lower early diastolic trough and a higher late diastolic peak. This also augmented the late systolic portion of the ascending aortic pressure waveform. Increasing compliance had

**Table 2. Comparison of the systolic/maximum and pulse pressure and velocity values as median (range) across various arteries from the YoungAdult model and the *in vivo* study (subject characteristics are given in Table 1)**

Artery	Pressure/velocity	Units	Model values	<i>In vivo</i> values
Ascending aorta	Pressure (systolic)	mmHg	105	102 (96–122)
	Pressure (pulse)	mmHg	25	35 (33–52)
Left common carotid artery	Pressure (systolic)	mmHg	111	102 (95–120)
	Pressure (pulse)	mmHg	32	37 (31–50)
	Velocity (maximum)	cm s <sup>-1</sup>	54	44 (38–89)
Left brachial artery	Velocity (pulse)	cm s <sup>-1</sup>	52	36 (30–69)
	Pressure (systolic)	mmHg	117	112 (105–126)
	Pressure (pulse)	mmHg	39	41 (34–56)
	Velocity (maximum)	cm s <sup>-1</sup>	35	49 (26–64)
Left radial artery	Velocity (pulse)	cm s <sup>-1</sup>	40	57 (34–79)
	Pressure (systolic)	mmHg	113	116 (114–145)
	Pressure (pulse)	mmHg	36	49 (45–75)
	Velocity (maximum)	cm s <sup>-1</sup>	30	20 (15–39)
Left superficial femoral artery	Velocity (pulse)	cm s <sup>-1</sup>	33	29 (21–43)
	Pressure (systolic)	mmHg	122	106 (98–127)
	Pressure (pulse)	mmHg	45	41 (30–57)
	Velocity (maximum)	cm s <sup>-1</sup>	36	37 (32–68)
Left posterior tibial artery	Velocity (pulse)	cm s <sup>-1</sup>	42	48 (32–89)
	Pressure (systolic)	mmHg	118	124 (114–134)
	Pressure (pulse)	mmHg	43	52 (43–68)
	Velocity (maximum)	cm s <sup>-1</sup>	36	21 (13–43)
Left superficial temporal artery	Velocity (pulse)	cm s <sup>-1</sup>	40	31 (18–59)
	Pressure (systolic)	mmHg	113	105 (94–129)
	Pressure (pulse)	mmHg	35	36 (30–59)

the opposite effect, with decreasing velocity and pressure amplitudes and reduced late systolic augmentation (Fig. 4).

A similar effect was seen when decreasing and increasing leg vascular bed compliance (Fig. 5).

Importantly, decreasing compliance augmented the diastolic hump of the ascending aortic pressure waveform, whereas increasing compliance had the opposite effect.

Increasing the cerebral vascular bed compliance also caused similar changes in the pressure waveforms of

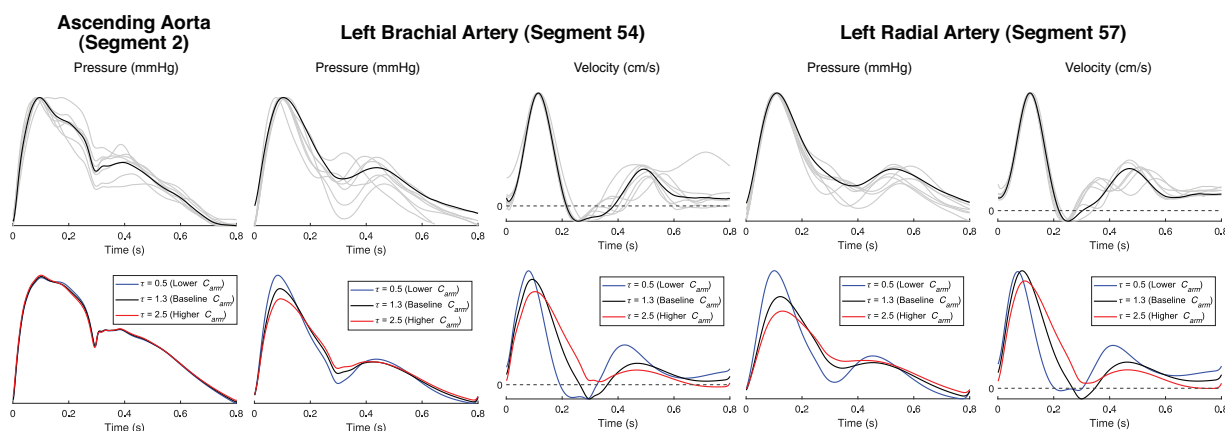


**Figure 4. Comparison of the ascending aortic, left brachial and left radial artery waveforms produced by the YoungAdult model (bottom panels) and *in vivo* data (top panels)**

The individual waveforms for each participant are shown in grey and the average waveform in black. The effect on the waveforms of varying the compliance of the arm vascular beds ( $C_{arm}$ ) by varying the time constant ( $\tau$ ) is also shown. The *in vivo* waveforms have been normalized for purposes of visualization. [Colour figure can be viewed at [wileyonlinelibrary.com](http://wileyonlinelibrary.com)]

the common carotid and superficial temporal arteries and slightly augmented the late systolic portion of the ascending aortic pressure waveform (Fig. 6).

**Wave reflection at the aorto-iliac bifurcation**

Introducing a reflection coefficient of 0.2 at the aorto-iliac bifurcation and adjusting the downstream leg vasculature

to maintain well-matched junctions thereafter affected the late systolic and diastolic portions of the ascending aortic pressure waveform and abolished the diastolic hump. It also increased the height of the diastolic notch (Fig. 7A) and masked the effect of changing leg vascular bed compliance on the ascending aortic pressure waveform, with decreasing compliance causing lesser modulation of the diastolic hump (Fig. 7B)

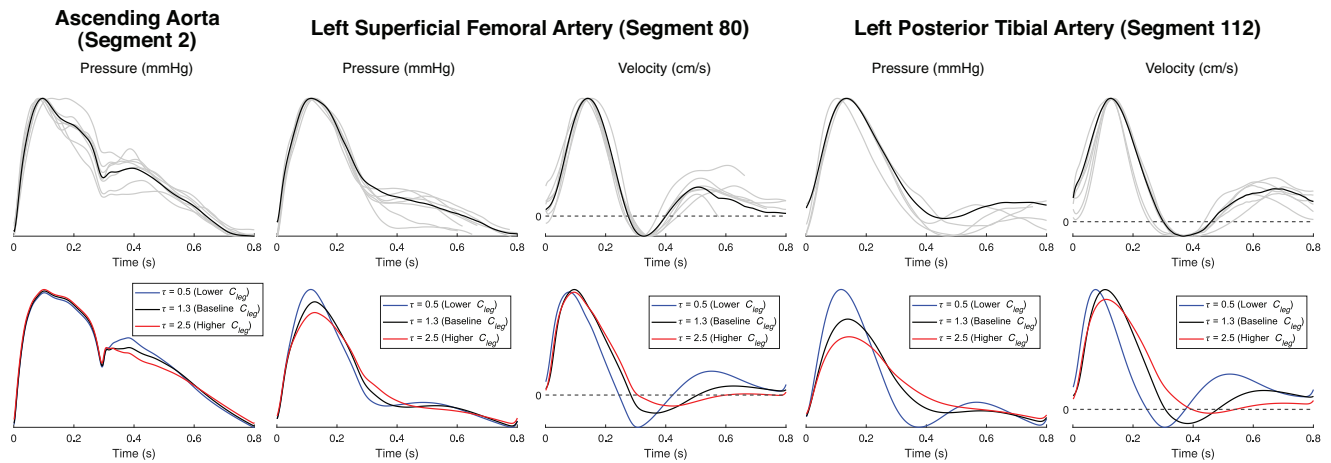


**Figure 5. Comparison of the ascending aortic, left superficial femoral and left posterior tibial artery waveforms produced by the YoungAdult (bottom panels) and *in vivo* data (top panels)**  
 The individual waveforms for each participant are shown in grey and the average waveform in black. The effect on the waveforms of varying the compliance of the leg vascular beds ( $C_{leg}$ ) by varying the time constant ( $\tau$ ) is also shown. The *in vivo* waveforms have been normalized for visualization. [Colour figure can be viewed at [wileyonlinelibrary.com](http://wileyonlinelibrary.com)]

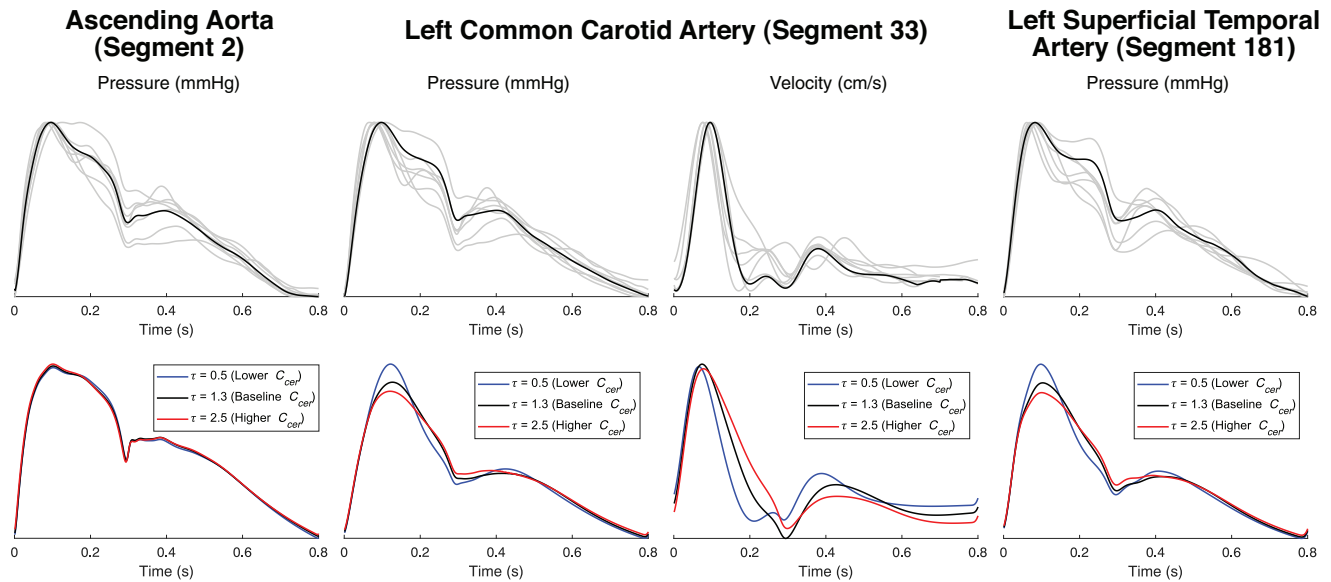


**Figure 6. Comparison of the ascending aortic, left common carotid and left superficial temporal artery waveforms produced by the YoungAdult model (bottom panels) and *in vivo* data (top panels)**  
 The individual waveforms for each participant are shown in grey and the average waveform in black. The effect on the waveforms of varying the compliance of the cerebral vascular beds ( $C_{cer}$ ) by varying the time constant ( $\tau$ ) is also shown. The *in vivo* waveforms have been normalized for visualization. The velocity profile of the superficial temporal artery was not measured. [Colour figure can be viewed at [wileyonlinelibrary.com](http://wileyonlinelibrary.com)]

when compared with the changes seen in Fig. 5 (where  $R_p = 0$ ).

### Impact of tapering on wave reflection

To investigate the impact of impedance-preserving vs. within-segment tapering on arterial wave reflection, Fig. 8 shows the effect of a large increase in  $C_{bed}$  that markedly reduced wave reflection in the distal vascular beds (thus revealing the contribution of wave reflection within the 1D network). In the Mynard2015 model (which includes substantial within-segment taper), the amplitude of  $P_{ref}$  (red) at the aorta was 29 mmHg at baseline and reduced by only 27% when  $C_{bed}$  was increased; there also remained a large difference between  $P$  (blue) and  $P_{in}$  (black in Fig. 8B). In contrast, the amplitude of  $P_{ref}$  in the ascending aorta of the YoungAdult model (with mostly impedance-preserving taper) was 17 mmHg at baseline (43% less than the Mynard2015 model) and reduced by 63% with increased  $C_{bed}$ ; the ascending aortic pressure and input waveforms also became very similar in shape (Fig. 8D), demonstrating that most of the wave reflection in the YoungAdult model arises at the level of the vascular beds.

### Discussion

In this study, we have described an optimized arterial network model that is the first to predict the characteristic features of the ascending aortic pressure waveform in young adults [early systolic peak, negative augmentation and a diastolic hump (Murgo et al., 1980; Nichols et al., 1985; O'Rourke & Hashimoto, 2007)] in addition to clearly triphasic velocity profiles in peripheral arteries.

The properties of the YoungAdult model that led to this improvement over earlier models were as follows: (i) an improved wave speed relationship that accounted for the degree of elasticity/muscularity of arteries in addition to their area; (ii) optimally matched junctions; (iii) impedance-preserving taper; and (iv) increased vascular bed compliance. Model results imply that the arterial network must be exquisitely well matched to exhibit the observed waveform features that are typical of healthy young adults, with minimal reflection of forward waves in the main conduit arteries (i.e. at junctions or owing to within-segment taper) and with reflection of forward waves occurring predominantly in the distal vascular beds. Furthermore, a major strength of our study is that both pressure and velocity waveforms produced by the model across major central and peripheral arteries were in close agreement with observed *in vivo* data measured in young adults.

We have proposed a novel empirical equation that uses both area and distance from the heart indexed to known transition points as a surrogate marker of the degree of elasticity/muscularity of an artery. Owing to the paucity of data on the wave speed of every artery, earlier studies have used different estimation techniques for the purpose of model parameterization. Westerhof et al. (1969) assigned an elastic modulus ( $E$ ) to each artery and calculated the wave speed using the Moens–Korteweg equation:  $c = \sqrt{Eh/2r\rho}$ , where  $\rho$  is blood density, and  $h$  and  $r$  are wall thickness and artery radius, respectively, using data from the study by Noordergraaf et al. (1963). Although the value of  $E$  increased in a stepwise manner ( $4 \times 10^6$ ,  $8 \times 10^6$  and  $16 \times 10^6$  g cm<sup>-1</sup> s<sup>-2</sup>) with increasing distance along an arterial path (Westerhof et al., 1969), the common carotid and femoral arteries were

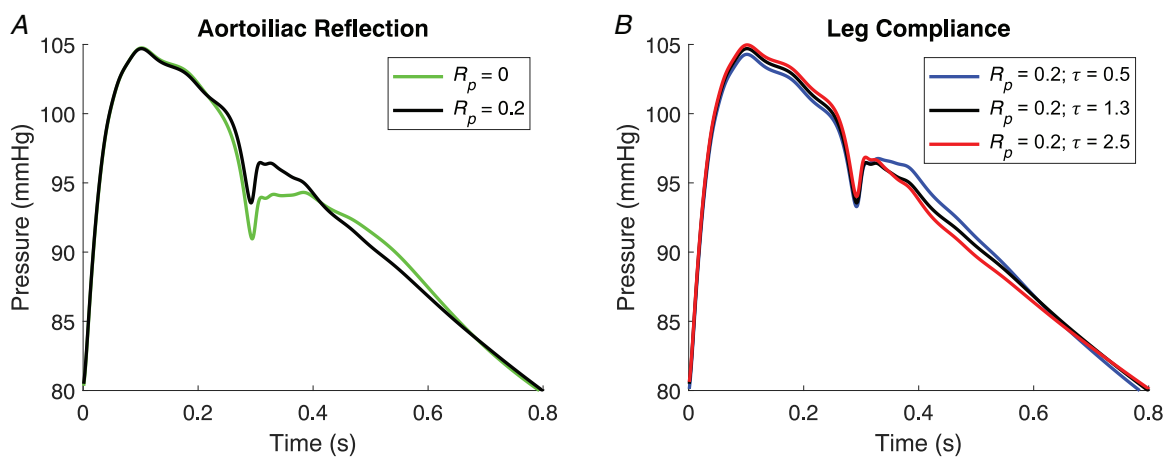


**Figure 7. Effect of aorto-iliac wave reflection on the ascending aortic pressure waveform**

A, comparison of the ascending aortic pressure waveform of the YoungAdult model with an aorto-iliac bifurcation reflection coefficient ( $R_p$ ) of 0 (baseline) and 0.2. B, effect of changing leg vascular bed compliance on the ascending aortic pressure waveform when aorto-iliac  $R_p = 0.2$ . [Colour figure can be viewed at [wileyonlinelibrary.com](http://wileyonlinelibrary.com)]

both assigned the same value of  $E$  ( $4 \times 10^6 \text{ g cm}^{-1} \text{ s}^{-2}$ ) and thus had similar wave speeds ( $582$  and  $625 \text{ cm s}^{-1}$ , respectively). This approach was also adopted by Stergiopoulos et al. (1992) and Avolio (1980), although Avolio increased the value of  $E$  for the femoral artery to  $8 \times 10^6 \text{ g cm}^{-1} \text{ s}^{-2}$ , which increased its wave speed to  $910 \text{ cm s}^{-1}$  and was therefore more representative of *in vivo* values.

To avoid the need to estimate  $E$  and  $h$  for every artery, Olufsen (1999) used data from the studies by Westerhof et al. (1969) and Stergiopoulos et al. (1992) to develop an empirical relationship between  $Eh/r$  and  $r$ . This allows the estimation of the wave speed of an artery based solely on its radius. This relationship has been used in multiple studies (Charlton et al., 2019;

Mynard & Smolich, 2015), although Reymond et al. (2009) later developed a similar empirical relationship based on published *in vivo* wave speeds. The drawback of these empirical relationships is that they provide similar wave speeds for arteries of similar radius but different wall properties (e.g. common carotid and femoral arteries). We have shown that our improved relationship provides substantially more accurate estimates of wave speed across a wide range of central and peripheral arteries in the young adult in comparison to previously used relationships, because it accounts for different wall properties as well as radius.

We incorporated impedance-preserving taper in the YoungAdult model, which moved the major reflection sites distally to the vascular beds. Many previous studies

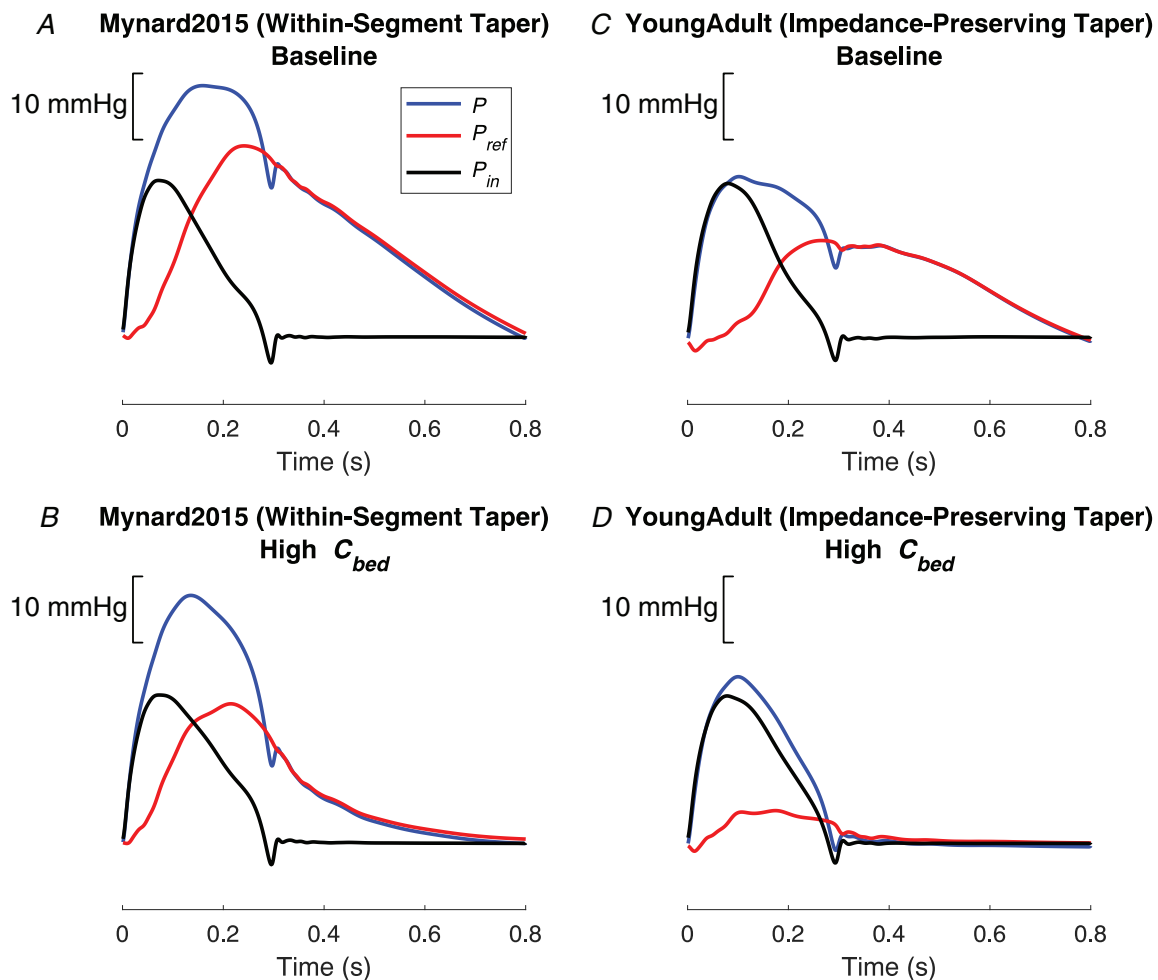


**Figure 8. Comparison of the effect of arterial taper and wave reflection on the ascending aortic pressure waveform**

The Mynard2015 model incorporated substantial within-segment taper (as in most other models), whereas the YoungAdult model eliminated within-segment taper by adding impedance-preserving side-branches. The total pressure ( $P$ ), input pressure ( $P_{in}$ ) and total reflected pressure ( $P_{ref}$ ) waveforms of the aorta are shown for the Mynard2015 and YoungAdult models with baseline vascular bed compliance ( $C_{bed}$ ) (A and C, respectively) and, to evaluate the influence of substantially reducing wave reflection from all distal vascular beds, with a 100-fold increase in  $C_{bed}$  (B and D, respectively). [Colour figure can be viewed at [wileyonlinelibrary.com](http://wileyonlinelibrary.com)]

have incorporated substantial within-segment taper [of up to 70% by area (Mynard & Smolich, 2015)] into cardiovascular models (Reymond et al., 2009; Stergiopoulos et al., 1992). Although arterial diameter is known to decrease with distance from the heart, Suwa et al. (1963) and Milnor and Bertram (1978) found little to no taper in sections of arteries between successive branching points. This led Papageorgiou & Jones (1987) to conclude that the reduction in diameter of an artery does not occur continuously (as assumed in previous models), but in steps, with each step occurring because of branching of the vascular tree. Implementing such impedance-preserving tapering in the YoungAdult model led to substantial changes in both central and peripheral arteries, compared with the Mynard2015 model (Mynard & Smolich, 2015), that resulted in an ascending aortic pressure waveform exhibiting the typical features of a young adult, in addition to triphasic velocity profiles in peripheral arteries.

Additional evidence for the lack of within-segment taper arises when considering model findings in Fig. 8 in light of experimental data presented by van den Bos et al. (1982). These authors found that substantial reduction of peripheral resistance and vascular bed wave reflection, via administration of the potent vasodilator sodium nitroprusside in dogs, led to pressure and flow waveforms in the ascending aorta having similar shapes. This indicated that vascular beds are likely to be the main sites of wave reflection. Our results are consistent with this conclusion, because increasing  $C_{bed}$  in the YoungAdult model produced similar pressure and flow waveforms in the ascending aorta (Fig. 8D) as in the study by van den Bos et al. (1982), noting that  $C_{bed}$  is likely to increase with vasodilatation. In contrast, even with a large increase in  $C_{bed}$  in the Mynard2015 model (that includes substantial within-segment taper), the ascending aortic pressure and flow waveforms still had dissimilar shapes, indicating that significant arterial wave reflection remained within the 1D network (i.e. conduit arteries).

Our findings therefore support the contention by Papageorgiou and Jones (1987) that 'true' arterial taper (i.e. within-segment taper) is unlikely to be a typical (or at least haemodynamically significant) feature in healthy young adults, and that vascular beds are the main sites of wave reflection in the vasculature (O'Rourke & Kelly, 1993). Indeed, from a design point of view, it is unclear why such within-segment taper would be beneficial. It was therefore not surprising that elimination of this impedance-increasing taper from the major arteries in the YoungAdult model caused wave reflection to occur more distally in the network, and caused the reflected waves to arrive in the ascending aorta during diastole. The reflected waves thus exerted minimal effect during systole (resulting in an early systolic peak and negative augmentation) but a prominent influence during diastole

(resulting in the diastolic hump), which is thought to be an optimal situation when considering cardiac energetics (O'Rourke & Hashimoto, 2007).

The influence of  $C_{bed}$  in 1D models has received little attention, but we observed that this parameter has a substantial effect on wave reflection properties in the vasculature. Importantly, we showed that the 'subtraction approach' to approximate  $C_{bed}$  might not provide accurate values, because calculated total arterial compliance (using model waveforms) is relatively insensitive to this quantity (Appendix C). Hence, we explored the effect of varying  $C_{bed}$  on velocity waveforms of distal arteries. Reflection from systemic vascular beds would produce a backward compression wave on wave intensity analysis (Mynard et al., 2020; Parker, 2009), the amplitude of which would be inversely related to  $C_{bed}$  (given that reducing  $C_{bed}$  increases reflection). The backward compression wave would decrease arterial flow (Parker, 2009), tending to produce backward flow and the triphasic velocity profiles seen in healthy conditions (Rangankar et al., 2016). This explains why decreasing  $C_{bed}$  (increased wave reflection) increased the triphasic nature of flow and caused earlier diastolic flow reversal, whereas increasing  $C_{bed}$  (reduced wave reflection) decreased it and made it more monophasic in nature. In fact, a monophasic velocity profile in distal arteries can point to a pathological condition, such as stenosis (Donnelly et al., 2000; Rangankar et al., 2016; Stergiopoulos et al., 1992). Previous models have produced monophasic femoral flow waveforms (Reymond et al., 2009; Stergiopoulos et al., 1992), suggesting that the  $C_{bed}$  values and/or vascular geometry might have been underestimated. Given that the precise value of  $C_{bed}$  is not currently known, our results suggest that the dominant effect of  $C_{bed}$  on the triphasic nature of velocity in distal arteries might be useful in guiding estimation of  $C_{bed}$ .

It is of interest that reduction of  $C_{bed}$  had a similar effect on both the pressure and velocity waveforms: increased early systolic peak, lower early diastolic trough and increased late systolic hump. This might be counter-intuitive, because a backward compression wave has opposite effects on pressure and velocity (Mynard et al., 2020; Parker, 2009). However, the similar effects of  $C_{bed}$  observed in conduit arteries are likely to be related to the fact that at arterial bifurcations, reflected waves from a given branch are transmitted into all other branches (not only the parent artery) (Mynard et al., 2017); therefore, they give rise to backward waves in addition to forward waves in peripheral arteries. Although the complex ensemble of reflected, re-reflected and transmitted waves makes it difficult to establish the basis for all waveform features precisely, changes in pressure and velocity that are in the same direction indicate a predominant effect of forward waves, whereas changes in the opposite direction indicate a predominant effect of backward waves.

Although it is known that the diastolic hump in the ascending aortic pressure waveform is caused by reflected waves arriving during diastole (O'Rourke & Yaginuma, 1984), the exact origin of these reflected waves is unclear. Based on *in vivo* experiments, O'Rourke and Taylor (1967) proposed that there were two distinct 'effective' reflection sites in the body, roughly corresponding to the upper and lower body. Consequently, they likened the systemic arterial network to an asymmetric T-tube model, with the shorter tube representing the upper body and the longer tube the lower body (O'Rourke, 1967). They also proposed that, in young adults, reflections from the upper body and lower body affect the early and later part of the cardiac cycle, respectively (O'Rourke & Avolio, 1980). Our simulations were consistent with this concept, given that increasing reflection from the arm/cerebral and leg arteries increased the late systolic portion and diastolic hump of the ascending aortic pressure waveform, respectively, thus providing insight into the effect of wave reflection from different regions of the body on the ascending aortic pressure waveform.

Given the clear influence of wave reflection from the legs on the diastolic hump (see Fig. 5), it was not surprising that this waveform feature was affected by the reflection properties of the aorto-iliac bifurcation. Although most arterial junctions appear to be well matched in the forward direction, the aorto-iliac bifurcation is thought to be a potential exception owing to observed lower daughter-to-parent area ratios (Papageorgiou et al., 1990). *Ex vivo* analysis of abdominal aortic and common iliac arteries by Greenwald et al. (1990) suggested that  $R_p$  at the aorto-iliac bifurcation might reach 0.2 or even higher in some young individuals, although most values in young adults were between 0 and 0.1. Our results show that introducing  $R_p = 0.2$  at the aorto-iliac bifurcation abolished the diastolic hump, indicating that the earlier wave reflection arriving at the aorta owing to the unmatched junction obscures the impact of reflection in the legs (as revealed by comparison with  $R_p = 0$ ; Figs 5 and 7). To achieve  $R_p = 0.2$ , all downstream vessels were reduced in diameter, thus increasing the characteristic impedance of all leg vessels. This would therefore reduce the impedance mismatch between the leg vessels and vascular beds, leading to lesser wave reflection in the legs. Consequently, one might view this change as 'transferring' some wave reflection to a more proximal location, leading to a reduced effective length of the arterial network. Our findings suggest that the aorto-iliac bifurcation (in addition to other arterial junctions in the lower body) might need to be well matched to obtain a prominent diastolic hump, although this needs to be investigated in future human studies. Interestingly, the effect of occluding

the femoral artery (mimicking an increased  $R_p$  at the aorto-iliac bifurcation) on the ascending aortic pressure waveform has shown mixed results; some studies have revealed a clear effect (Latham et al., 1985; Murgo et al., 1980), whereas others have not (Baksi et al., 2016; Khir & Parker, 2005). Thus, this warrants further investigation.

There are some limitations that should be considered when interpreting the results of the present study. First, for simplicity and consistency, a single value of  $\tau = 1.3$  was used for all vascular beds. Although this produced acceptable waveforms in all arteries, we did observe that using  $\tau = 0.5$  in only the arm vascular beds (with  $\tau = 1.3$  in all other beds) produced arm waveforms that were closer to those obtained *in vivo* compared with the baseline model (Fig. 4); however, using  $\tau = 0.5$  in all vascular beds abolished the early systolic peak and negative augmentation in the ascending aortic pressure waveform. Thus, future studies could investigate methods for estimating  $C_{bed}$  of individual vascular beds more precisely. Second, obtaining the ascending aortic pressure waveform directly was beyond the scope of the study; hence, it had to be estimated using a transfer function applied to the carotid pressure waveform, which could potentially reduce the accuracy of the *in vivo* systolic and pulse pressure values obtained for the ascending aorta. Although the resulting ascending aortic pulse pressure was lower than that calculated in our cohort, the value obtained was within the normal range compared with literature data (McEniery et al., 2005).

In conclusion, we have shown that the YoungAdult systemic arterial network model incorporating more accurate arterial wave speeds, impedance-preserving taper and well-matched junctions exhibits reflected waves that arise predominantly at the level of the vascular beds and arrive in the ascending aorta during the diastolic period. These physiological features produce waveform features that are typical of a healthy young adult, including an early systolic peak, negative augmentation and a diastolic hump in the ascending aorta, in addition to triphasic velocity profiles in peripheral arteries. Our model provides new insights into the 'fine-tuning' of arterial network properties, and it can be used as a baseline in future studies of cardiovascular ageing and disease.

## Appendix A: improved wave speed relationship

Table A1 shows the wave speed values from literature that were used to guide the development of the area- and transition distance index-dependent wave speed relationship used in the YoungAdult model.

**Table A1. Wave speed values of various arteries extracted from literature. Segment numbers refer to Fig. 2 in the main manuscript, and area and transition distance index refer to model-based values. Average wave speeds are the final values used to develop the wave speed relationship.**

Segment number	Vessel name	Area (cm <sup>2</sup> )	Transition distance index	Wave speed (cm s <sup>-1</sup> ) (reference)	Average wave speed (cm s <sup>-1</sup> )
2	Ascending aorta	5.94	0.022	357 (Redheuil et al., 2010) <sup>§</sup> 374 (Petersen et al., 2006) <sup>§</sup> 364 (Rider et al., 2012) <sup>§</sup> 370 (Kim et al., 2013) <sup>¶</sup>	366
6	Right common carotid artery	0.40	0.447	458 (Rakobowchuk et al., 2008) <sup>#</sup> 426 (Jourdan et al., 2005) <sup>#</sup> 485 (Engelen et al., 2015) <sup>#</sup> 397 (Mikola et al., 2015) <sup>#</sup> 424 (Petersen et al., 2006) <sup>§</sup>	438
32	Aortic arch II	4.69	0.154	390 (Hickson et al., 2010) <sup>¶</sup> 420 (Kröner et al., 2013) <sup>¶</sup>	405
38	Descending thoracic aorta I	4.00	0.240	362 (Redheuil et al., 2010) <sup>§</sup> 440 (Petersen et al., 2006) <sup>§</sup> 410 (Rider et al., 2012) <sup>§</sup> 459 (Kim et al., 2013) <sup>§</sup> 430 (Hickson et al., 2010) <sup>¶</sup> 490 (Kröner et al., 2013) <sup>¶</sup>	432
46	Left axillary artery II	0.39	0.945	481 (Bjarnegård & Länne, 2010) <sup>#</sup>	481
48	Left brachial artery I	0.37	1	801 (Bjarnegård & Länne, 2010) <sup>#</sup>	801
54	Left brachial artery IV	0.14	2.261	904 (Salzer et al., 2008) <sup>#</sup> 991 (De Hoon et al., 2003) <sup>#</sup> 1107 (Bjarnegård & Länne, 2010) <sup>#</sup>	1001
57	Left radial artery II	0.04	3.13	1069 (Giannattasio et al., 2001) <sup>#</sup> 1007*	1038
62	Descending thoracic aorta II	2.68	0.355	424 (Groenink et al., 1998) <sup>§</sup> 467 (Kim et al., 2013) <sup>§</sup> 405 (Kim et al., 2013) <sup>¶</sup> 360 (Devos et al., 2015) <sup>¶</sup> 446 (Rogers et al., 2001) <sup>¶</sup> 570 (Latham et al., 1985) <sup>†</sup> 480 (Kim et al., 2013) <sup>¶</sup> 440 (Hickson et al., 2010) <sup>¶</sup> 360 (Devos et al., 2015) <sup>¶</sup>	439
73	Abdominal aorta IV	1.40	0.744	480 (Devos et al., 2015) <sup>¶</sup> 514 (Rogers et al., 2001) <sup>¶</sup> 470 (Kim et al., 2013) <sup>¶</sup> 450 (Hickson et al., 2010) <sup>¶</sup> 510 (Kröner et al., 2013) <sup>¶</sup> 430 (Devos et al., 2015) <sup>¶</sup>	476
76	Left common iliac artery	1.31	1	880 (Latham et al., 1985) <sup>†</sup>	880
80	Left femoral artery I	0.42	1.449	926 (van den Berkmortel et al., 1998) <sup>#</sup> 1029 (Bossuyt et al., 2015) <sup>#</sup> 709 (Rakobowchuk et al., 2009) <sup>#</sup> 957 (De Hoon et al., 2003) <sup>#</sup>	905
94	Left popliteal artery I	0.22	2.154	916 (Rakobowchuk et al., 2008) <sup>#</sup>	916

The vessel names and segment numbers correspond to the vessel names in Supplemental File 1.

<sup>§</sup>Calculated via reported distensibility measured using magnetic resonance imaging (MRI) and  $c = \sqrt{(1/\rho D)}$ , where  $c$  is wave speed,  $\rho$  is density, and  $D$  is distensibility.

<sup>¶</sup>Calculated via the transit time between two sections a known distance apart using MRI.

<sup>#</sup>Calculated via reported distensibility measured using ultrasonography using  $c = \sqrt{(1/\rho D)}$ .

\*Calculated using transit time from the validation portion of this study using applanation tonometry and electrocardiography. Arrival time at the distal end of the brachial and radial arteries was calculated as the time difference between the peak of the QRS complex of the ECG and the upstroke of the pressure waveform obtained using applanation tonometry. The transit time was taken as the difference between the arrival times of the distal ends of the radial and brachial arteries. Finally, the radial wave speed was estimated by measuring the distance between the tonometry sites.

<sup>†</sup>Calculated via the transit time between two sections a known distance apart using simultaneous invasive micromanometer measurements.



## Appendix B: model formulation

### Governing equations

The equations governing haemodynamics in the YoungAdult model were the 1D Navier–Stokes equations derived from the laws of conservation of mass and momentum (Sherwin et al., 2003; Streeter et al., 1963), as follows:

$$\frac{\partial A}{\partial t} + \frac{\partial Au}{\partial x} = 0 \quad (\text{B1})$$

and

$$\frac{\partial u}{\partial t} + u \frac{\partial u}{\partial x} + \frac{1}{\rho} \frac{\partial P}{\partial x} = f, \quad (\text{B2})$$

where  $A$  is area,  $u$  is velocity,  $P$  is pressure,  $\rho$  is blood density ( $1.06 \text{ g cm}^{-3}$ ), and  $f = -\xi\pi\mu u/A$ , where  $\xi$  was calculated using the model described by Bessems et al. (2007). Additionally, a wall law was implemented that governed the relationship between pressure and area:

$$P - P_{\text{ext}} = \frac{2\rho c_0^2}{b} \left[ \left( \frac{A}{A_0} \right)^{\frac{b}{2}} - 1 \right] + \frac{\Gamma}{A\sqrt{A}} \frac{\partial A}{\partial t} + P_0, \quad (\text{B3})$$

$$b = \frac{2\rho c_0^2}{P_0 - P_{\text{collapse}}} \quad (\text{B4})$$

and

$$\Gamma = \frac{b_1}{D} + b_0, \quad (\text{B5})$$

where  $P_{\text{ext}}$  is external pressure (assumed to be zero),  $P_{\text{collapse}}$  is a nominal pressure at which  $A \rightarrow 0$  [taken as  $-10 \text{ mmHg}$  (Langewouters et al., 1984)],  $P_0$  is a reference pressure (taken to be  $80 \text{ mmHg}$ ),  $c_0$  is the wave speed at  $P_0$ ,  $A_0$  is the area at  $P_0$ ,  $\Gamma$  is a coefficient of wall viscosity,  $D$  is vessel diameter,  $b_1 = 100 \text{ g cm s}^{-1}$ , and  $b_0 = 400 \text{ g s}^{-1}$  (Mynard & Smolich, 2015).

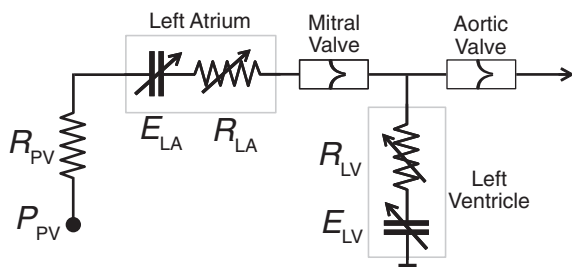


Figure B1. Schematic diagram of the left-heart model

### Two-chamber elastance heart model

The two-chamber left-heart model shown in Fig. B1 was used in all presented simulations; it consisted of the left atrium and ventricle, mitral and aortic valves, a pulmonary venous resistance ( $R_{\text{PV}} = 0.05 \text{ mmHg s ml}^{-1}$ )

Table B1. Values of parameters for the left-heart model

Parameter	Symbol	Units	Left atrium	Left ventricle
Maximal elastance	$E_{\text{max}}$	mmHg ml <sup>-1</sup>	0.13	2.48
Minimal elastance	$E_{\text{min}}$	mmHg ml <sup>-1</sup>	0.09	0.07
Systolic time constant	$\tau_1$	s	0.053	0.269
Diastolic time constant	$\tau_2$	s	0.172	0.452
Contraction rate constant	$m_1$	—	1.99	1.32
Relaxation rate constant	$m_2$	—	11.2	21.9
Residual volume	$V_{p=0}$	ml	3.0	10.0
Initial volume	$V_{t=0}$	ml	15.8	158.0
Source resistance coefficient	$K_s$	$\times 10^{-4} \text{ s ml}^{-1}$	2.5	5.0
Onset of contraction	—	s	0.8125	0.0

Table B2. Parameter values for the mitral and aortic valve models

Parameter	Symbol	Units	Mitral valve	Aortic valve
Opening pressure coefficient	$K_{\text{vo}}$	—	0.02	0.02
Closure pressure coefficient	$K_{\text{vc}}$	—	0.04	0.02
Annular area	$A_{\text{ann}}$	cm <sup>2</sup>	5.1	4.9

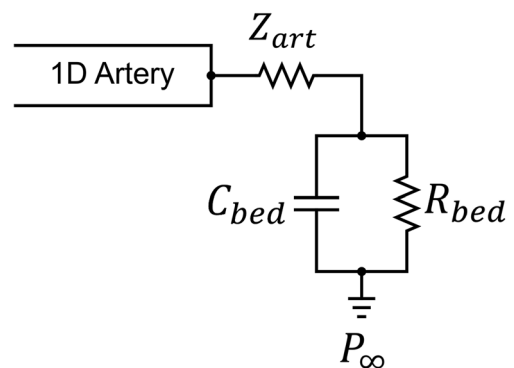


Figure B2. Schematic diagram of a one-dimensional artery terminating in a vascular bed (Windkessel model)

and a constant pulmonary venous pressure ( $P_{pV} = 10.8$  mmHg). The left atrium and ventricle were modelled as time-varying elastance chambers ( $E_{LA}$  and  $E_{LV}$ , respectively), with source resistance ( $R_{LA}$  and  $R_{LV}$ , respectively), as described by Mynard (2011). Heart rate was set to  $75 \text{ beats min}^{-1}$ .

The parameters  $E_{LA}$  and  $E_{LV}$  are defined by two Hill functions using the following parameters:  $E_{max}$ ,  $E_{min}$ ,  $\tau_1$ ,  $\tau_2$ ,  $m_1$ ,  $m_2$ ,  $V_p = 0$  and  $V_t = 0$ ;  $R_{LA}$  and  $R_{LV}$  are related to  $E_{LA}$  and  $E_{LV}$ , respectively, via a source resistance coefficient,  $K_s$  [see Mynard (2011) for further details]. The values of these parameters for this study are given in Table B1.

The pressure–flow relationship of the mitral and aortic valves (with annulus area,  $A_{ann}$ ) was described by the

Bernoulli equation, and the opening/closing dynamics were governed by the valve opening and valve closing rate coefficients,  $K_{vo}$  and  $K_{vc}$  (Table B2) (Mynard et al., 2012).

### Vascular bed model

All terminal 1D arteries were connected to three-element Windkessel compartments, which included two resistance elements [characteristic impedance of the terminal 1D artery ( $Z_{art}$ ) and peripheral resistance of the vascular bed ( $R_{bed}$ )] and one capacitor element ( $C_{bed}$ ) that represents the compliance of the vascular bed (Fig. B2). The venous system is represented as a constant outlet pressure ( $P_{\infty}$ ) of 5 mmHg. The  $Z_{art}$  was matched to

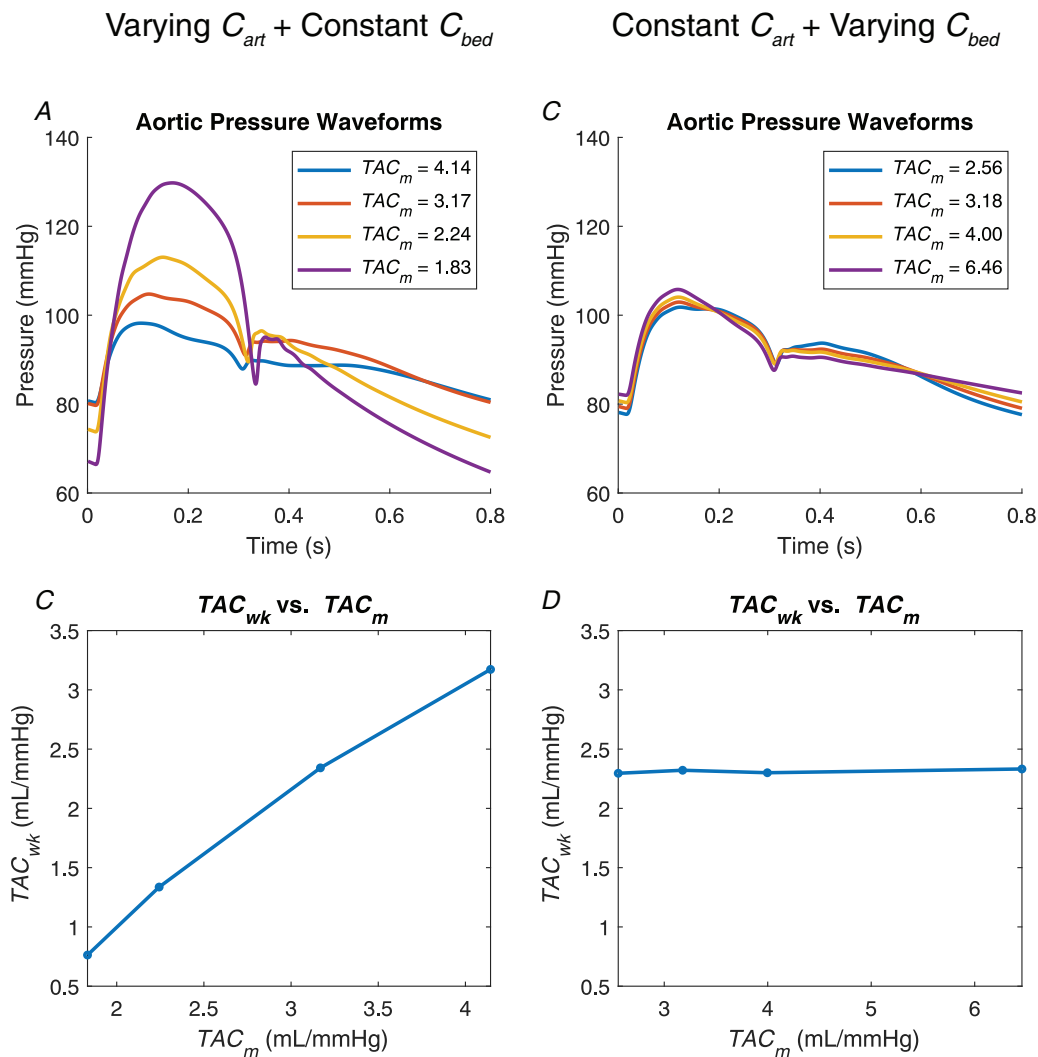


**Figure C1. Differing effects of vascular bed compliance and arterial compliance on total arterial compliance**

A, aortic pressure waveforms obtained by keeping vascular bed compliance ( $C_{bed}$ ) constant but changing arterial compliance ( $C_{art}$ ). B, corresponding values of total arterial compliance obtained using the Windkessel pulse pressure method ( $TAC_{wk}$ ) vs. that of the YoungAdult model ( $TAC_m$ ). C, aortic pressure waveforms obtained by keeping  $C_{art}$  constant and changing  $C_{bed}$ . D, corresponding values of  $TAC_{wk}$  vs.  $TAC_m$ . [Colour figure can be viewed at [wileyonlinelibrary.com](http://wileyonlinelibrary.com)]

the characteristic impedance of the 1D artery to prevent non-physiological reflection of higher-frequency wave components (Alastruey et al., 2008; Stergiopoulos et al., 1992). For more detail, please refer to Mynard (2011).

## Appendix C: Windkessel compliance

We wanted to investigate whether the two-element Windkessel pulse pressure method (Stergiopoulos et al., 1994) to estimate total arterial compliance ( $TAC_{wk}$ ) was sensitive to both conduit arterial ( $C_{art}$ ) and vascular bed compliance ( $C_{bed}$ ). To this end, we performed two experiments using the YoungAdult model: experiment 1, keeping  $C_{bed}$  of all beds constant and progressively decreasing  $C_{art}$  by multiplying the wave speed of every vessel by a factor (thus maintaining the junction matching); and experiment 2, keeping  $C_{art}$  constant and progressively increasing  $C_{bed}$  of all beds by the same factor. For each scenario, we calculated the total compliance of every vessel and vascular bed in the YoungAdult model ( $TAC_m$ ) that is precisely known and compared it with the corresponding  $TAC_{wk}$  using the aortic pressure and flow waveforms produced by the model.

As seen in Fig. C1A, when only  $C_{art}$  was decreased but  $C_{bed}$  was kept constant (experiment 1), the aortic pulse pressure increased with a decrease in  $C_{art}$  (and consequently,  $TAC_m$ ), with a range of 17–65 mmHg. There was also a good correlation between  $TAC_{wk}$  and  $TAC_m$  when only  $C_{art}$  was decreased but  $C_{bed}$  was kept constant; a 56% reduction in  $TAC_m$  corresponded to a 76% reduction in  $TAC_{wk}$  (Fig. C1B). In contrast, although there was a significant change in the shape of the aortic pressure waveform with an increase in  $C_{bed}$  (and consequently, an increase in  $TAC_m$ ) but constant  $C_{art}$  (experiment 2), there was not much change in its pulse pressure, with a range of only 24–26 mmHg (Fig. C1C). There was also very little change in  $TAC_{wk}$  with increasing  $TAC_m$ ; even an increase in  $TAC_m$  by 153% corresponded to only a 1.6% increase in  $TAC_{wk}$ . These results suggest that although  $TAC_{wk}$  is sensitive to  $C_{art}$ , it is insensitive to  $C_{bed}$ . This is because  $TAC_{wk}$  is entirely dependent on the aortic pulse pressure, which is affected mostly by  $C_{art}$  but not significantly by  $C_{bed}$ .

## References

- Alastruey, J., Parker, K., Peiró, J., & Sherwin, S. (2008). Lumped parameter outflow models for 1-d blood flow simulations: Effect on pulse waves and parameter estimation. *Communications in Computational Physics*, **4**, 317–336.
- Alastruey, J., Parker, K., Peiró, J., & Sherwin, S. (2009). Analysing the pattern of pulse waves in arterial networks: A time-domain study. *Journal of Engineering Mathematics*, **64**(4), 331–351.
- Avolio, A. (1980). Multi-branched model of the human arterial system. *Medical & Biological Engineering & Computing*, **18**(6), 709–718.
- Baksi, A. J., Davies, J. E., Hadjiloizou, N., Baruah, R., Unsworth, B., Foale, R. A., Korolkova, O., Siggers, J. H., Francis, D. P., & Mayet, J. (2016). Attenuation of reflected waves in man during retrograde propagation from femoral artery to proximal aorta. *International Journal of Cardiology*, **202**, 441–445.
- Beniwal, S., Bhargava, K., & Kausik, S. K. (2014). Size of distal radial and distal ulnar arteries in adults of southern rajasthan and their implications for percutaneous coronary interventions. *Indian Heart Journal*, **66**(5), 506–509.
- Bessemers, D., Rutten, M., & Van De Vosse, F. (2007). A wave propagation model of blood flow in large vessels using an approximate velocity profile function. *Journal of Fluid Mechanics*, **580**, 145–168.
- Betts, J. G., Desaix, P., Johnson, E., Johnson, J. E., Korol, O., Kruse, D., Poe, B., Wise, J. A., Womble, M., & Young, K. A. (2013). *Anatomy & physiology*. OpenStax College, Rice University.
- Bjarnegård, N., & Länne, T. (2010). Arterial properties along the upper arm in humans: Age-related effects and the consequence of anatomical location. *Journal of Applied Physiology (Bethesda, Md : 1985)*, **108**(1), 34–38.
- Black, C. D., Vickerson, B., & McCully, K. K. (2003). Non-invasive assessment of vascular function in the posterior tibial artery of healthy humans. *Dynamic Medicine: DM*, **2**(1), 1.
- Blanco, P., Watanabe, S., Passos, M., Lemos, P., & Feijoo, R. (2014). An anatomically detailed arterial network model for one-dimensional computational hemodynamics. *Ieee Transactions on Bio-Medical Engineering*, **62**(2), 736–753.
- Bossuyt, J., Engelen, L., Ferreira, I., Stehouwer, C. D., Boutouyrie, P., Laurent, S., Segers, P., Reesink, K., Van Bortel, L. M. & Collaboration obotRVfAM (2015). Reference values for local arterial stiffness. Part B: Femoral artery. *Journal of Hypertension*, **33**(10), 1997–2009.
- Brandfonbrener, M., Landowne, M., & Shock, N. W. (1955). Changes in cardiac output with age. *Circulation*, **12**(4), 557–566.
- Charlton, P. H., Mariscal Harana, J., Vennin, S., Li, Y., Chowienczyk, P., & Alastruey, J. (2019). Modeling arterial pulse waves in healthy aging: A database for in silico evaluation of hemodynamics and pulse wave indexes. *American Journal of Physiology Heart and Circulatory Physiology*, **317**(5), H1062–H1085.
- Chen, C.-H., Ting, C.-T., Nussbacher, A., Nevo, E., Kass, D. A., Pak, P., Wang, S.-P., Chang, M.-S., & Yin, F. C. P. (1996). Validation of carotid artery tonometry as a means of estimating augmentation index of ascending aortic pressure. *Hypertension*, **27**(2), 168–175.
- Chirinos, J. A., Kips, J. G., Jacobs, D. R., Brumback, L., Duprez, D. A., Kronmal, R., Bluemke, D. A., Townsend, R. R., Vermeersch, S., & Segers, P. (2012a). Arterial wave reflections and incident cardiovascular events and heart failure: Mesa (multiethnic study of atherosclerosis). *Journal of the American College of Cardiology*, **60**(21), 2170–2177.

- Chirinos, J. A., Segers, P., Gillebert, T. C., Gupta, A. K., De Buyzere, M. L., De Bacquer, D., St John-Sutton, M., & Rietzschel, E. R. (2012b). Arterial properties as determinants of time-varying myocardial stress in humans. *Hypertension*, **60**(1), 64–70.
- De Hoon, J., Willigers, J., Troost, J., Struijker-Boudier, H., & Van Bortel, L. (2003). Cranial and peripheral interictal vascular changes in migraine patients. *Cephalalgia*, **23**(2), 96–104.
- Devos, D. G., Rietzschel, E., Heyse, C., Vandemaele, P., Van Bortel, L., Babin, D., Segers, P., Westenberg, J. M., & Achten, R. (2015). Mr pulse wave velocity increases with age faster in the thoracic aorta than in the abdominal aorta. *Journal of Magnetic Resonance Imaging*, **41**(3), 765–772.
- Donnelly, R., Hinwood, D., & London, N. J. (2000). Abc of arterial and venous disease. Non-invasive methods of arterial and venous assessment. *BMJ*, **320**(7236), 698–701.
- Engelen, L., Bossuyt, J., Ferreira, I., van Bortel, L. M., Reesink, K. D., Segers, P., Stehouwer, C. D., Laurent, S., & Boutouyrie, P. (2015). Reference values for local arterial stiffness. Part a: Carotid artery. *Journal of Hypertension*, **33**(10), 1981–1996.
- Gerhard-Herman, M., Gardin, J. M., Jaff, M., Mohler, E., Roman, M., & Naqvi, T. Z. (2006). Guidelines for non-invasive vascular laboratory testing: A report from the american society of echocardiography and the society for vascular medicine and biology. *Vascular Medicine*, **11**(3), 183–200.
- Giannattasio, C., Failla, M., Grappiolo, A., Calchera, I., Grieco, N., Carugo, S., Bigoni, M., Randelli, P., Peretti, G., & Mancina, G. (2001). Effects of physical training of the dominant arm on ipsilateral radial artery distensibility and structure. *Journal of Hypertension*, **19**(1), 71–77.
- Greenwald, S. E., Carter, A. C., & Berry, C. L. (1990). Effect of age on the in vitro reflection coefficient of the aortoiliac bifurcation in humans. *Circulation*, **82**(1), 114–123.
- Groenink, M., de Roos, A., Mulder, B. J., Spaan, J. A., & van der Wall, E. E. (1998). Changes in aortic distensibility and pulse wave velocity assessed with magnetic resonance imaging following beta-blocker therapy in the marfan syndrome. *American Journal of Cardiology*, **82**(2), 203–208.
- Hamilton, W. F. (1944). The patterns of the arterial pressure pulse. *American Journal of Physiology*, **141**(2), 235–241.
- Hansen, K. W., & Orskov, H. (1992). A plea for consistent reliability in ambulatory blood pressure monitors: A reminder. *Journal of Hypertension*, **10**(11), 1313–1315.
- Hickson, S. S., Butlin, M., Graves, M., Taviani, V., Avolio, A. P., McEniery, C. M., & Wilkinson, I. B. (2010). The relationship of age with regional aortic stiffness and diameter. *JACC Cardiovasc Imaging*, **3**(12), 1247–1255.
- Hwang, J. Y. (2017). Doppler ultrasonography of the lower extremity arteries: Anatomy and scanning guidelines. *Ultrasonography*, **36**(2), 111–119.
- Jourdan, C., Wühl, E., Litwin, M., Fahr, K., Trelewicz, J., Jobs, K., Schenk, J. P., Grenda, R., Mehls, O., Tröger, J., & Schaefer, F. (2005). Normative values for intima-media thickness and distensibility of large arteries in healthy adolescents. *Journal of Hypertension*, **23**(9), 1707–1715.
- Katori, R. (1979). Normal cardiac output in relation to age and body size. *The Tohoku Journal of Experimental Medicine*, **128**(4), 377–387.
- Kelly, R., & Fitchett, D. (1992). Noninvasive determination of aortic input impedance and external left ventricular power output: A validation and repeatability study of a new technique. *Journal of the American College of Cardiology*, **20**(4), 952–963.
- Kelly, R., Hayward, C., Avolio, A., & O'Rourke, M. (1989). Noninvasive determination of age-related changes in the human arterial pulse. *Circulation*, **80**(6), 1652–1659.
- Khair, A. W., & Parker, K. H. (2005). Wave intensity in the ascending aorta: Effects of arterial occlusion. *Journal of Biomechanics*, **38**(4), 647–655.
- Kim, E. K., Chang, S. A., Jang, S. Y., Kim, Y., Kim, S. M., Oh, J. K., Choe, Y. H., & Kim, D. K. (2013). Assessment of regional aortic stiffness with cardiac magnetic resonance imaging in a healthy asian population. *The International Journal of Cardiovascular Imaging*, **29**(S1), 57–64.
- Kim, E. S., Sharma, A. M., Scissons, R., Dawson, D., Eberhardt, R. T., Gerhard-Herman, M., Hughes, J. P., Knight, S., Marie Kupinski, A., Mahe, G., Neumyer, M., Poe, P., Shugart, R., Wennberg, P., Williams, D. M., & Zierler, R. E. (2020). Interpretation of peripheral arterial and venous doppler waveforms: A consensus statement from the society for vascular medicine and society for vascular ultrasound. *Vascular Medicine*, **25**(5), 484–506.
- Kondiboyina, A., Smolich, J. J., Cheung, M. M. H., Westerhof, B. E., & Mynard, J. P. (2020). Conduit arterial wave reflection promotes pressure transmission but impedes hydraulic energy transmission to the microvasculature. *American Journal of Physiology Heart and Circulatory Physiology*, **319**(1), H66–H75.
- Kröner, E. S., Scholte, A. J., de Koning, P. J., van den Boogaard, P. J., Kroft, L. J., van der Geest, R. J., Hilhorst-Hofstee, Y., Lamb, H. J., Siebelink, H. M., Mulder, B. J., Groenink, M., Radonic, T., van der Wall, E. E., de Roos, A., Reiber, J. H., & Westenberg, J. J. (2013). MRI-assessed regional pulse wave velocity for predicting absence of regional aorta luminal growth in marfan syndrome. *International Journal of Cardiology*, **167**(6), 2977–2982.
- Langewouters, G. J., Wesseling, K. H., & Goedhard, W. J. A. (1984). The static elastic properties of 45 human thoracic and 20 abdominal aortas in vitro and the parameters of a new model. *Journal of Biomechanics*, **17**(6), 425–435.
- Latham, R. D., Westerhof, N., Sipkema, P., Rubal, B. J., Reuderink, P., & Murgu, J. P. (1985). Regional wave travel and reflections along the human aorta: A study with six simultaneous micromanometric pressures. *Circulation*, **72**(6), 1257–1269.
- Leaoyd, B. M., & Taylor, M. G. (1966). Alterations with age in the viscoelastic properties of human arterial walls. *Circulation Research*, **18**(3), 278–292.
- Lee, H. Y., & Oh, B. H. (2010). Aging and arterial stiffness. *Circulation Journal*, **74**(11), 2257–2262.
- Leloup, A. J., Van Hove, C. E., Heykers, A., Schrijvers, D. M., De Meyer, G. R., & Franssen, P. (2015). Elastic and muscular arteries differ in structure, basal no production and voltage-gated ca(2+)-channels. *Frontiers in Physiology*, **6**, 375.

- Lockwood, G. R., Ryan, L. K., Gotlieb, A. I., Lonn, E., Hunt, J. W., Liu, P., & Foster, F. S. (1992). In vitro high resolution intravascular imaging in muscular and elastic arteries. *Journal of the American College of Cardiology*, **20**(1), 153–160.
- Lorbeer, R., Grotz, A., Dörr, M., Völzke, H., Lieb, W., Kühn, J. P., & Mensel, B. (2018). Reference values of vessel diameters, stenosis prevalence, and arterial variations of the lower limb arteries in a male population sample using contrast-enhanced mr angiography. *PLoS One*, **13**(6), e0197559.
- Maixner, W., Wright, C. B., Schoepfle, W. J., & Barnes, R. W. (1980). Femoral artery flow velocities: A sensitive index of limb hemodynamics associated with venous occlusion. *Journal of Surgical Research*, **29**(4), 326–330.
- Master, A. M., Dublin, L. I., & Marks, H. H. (1950). The normal blood pressure range and its clinical implications. *Journal of the American Medical Association*, **143**(17), 1464–1470.
- McEniery, C. M., Yasmin, Hall, I. R., Qasem, A., Wilkinson, I. B., & Cockcroft, J. R. (2005). Normal vascular aging: Differential effects on wave reflection and aortic pulse wave velocity: The anglo-cardiff collaborative trial (ACCT). *Journal of the American College of Cardiology*, **46**(9), 1753–1760.
- Mikola, H., Pahlkala, K., Rönnemaa, T., Viikari, J. S. A., Niinikoski, H., Jokinen, E., Salo, P., Simell, O., Juonala, M., & Raitakari, O. T. (2015). Distensibility of the aorta and carotid artery and left ventricular mass from childhood to early adulthood. *Hypertension*, **65**(1), 146–152.
- Milnor, W. R., & Bertram, C. D. (1978). The relation between arterial viscoelasticity and wave propagation in the canine femoral artery in vivo. *Circulation Research*, **43**(6), 870–879.
- Murgo, J. P., Westerhof, N., Giolma, J. P., & Altobelli, S. A. (1980). Aortic input impedance in normal man: Relationship to pressure wave forms. *Circulation*, **62**(1), 105–116.
- Mynard, J. P. (2011). Computer modelling and wave intensity analysis of perinatal cardiovascular function and dysfunction. PhD Thesis, University of Melbourne.
- Mynard, J. P., Davidson, M. R., Penny, D. J., & Smolich, J. J. (2012). A simple, versatile valve model for use in lumped parameter and one-dimensional cardiovascular models. *International Journal for Numerical Methods in Biomedical Engineering*, **28**(6-7), 626–641.
- Mynard, J. P., Kondiboyina, A., Kowalski, R., Cheung, M. M. H., & Smolich, J. J. (2020). Measurement, analysis and interpretation of pressure/flow waves in blood vessels. *Frontiers in Physiology*, **11**, 1085.
- Mynard, J. P., Kowalski, R., Cheung, M. M. H., & Smolich, J. J. (2017). Beyond the aorta: Partial transmission of reflected waves from aortic coarctation into supra-aortic branches modulates cerebral hemodynamics and left ventricular load. *Biomechanics and Modeling in Mechanobiology*, **16**(2), 635–650.
- Mynard, J. P., & Nithiarasu, P. (2008). A 1d arterial blood flow model incorporating ventricular pressure, aortic valve and regional coronary flow using the locally conservative galerkin (lcg) method. *Communications in Numerical Methods in Engineering*, **24**(5), 367–417.
- Mynard, J. P., & Smolich, J. J. (2015). One-dimensional haemodynamic modeling and wave dynamics in the entire adult circulation. *Annals of Biomedical Engineering*, **43**(6), 1443–1460.
- Negoita, M., Hughes, A. D., Parker, K. H., & Khir, A. W. (2018). A method for determining local pulse wave velocity in human ascending aorta from sequential ultrasound measurements of diameter and velocity. *Physiological Measurement*, **39**(11), 114009.
- Nichols, W. W. (1998). *McDonald's blood flow in arteries: Theoretical, experimental, and clinical principles /wilmer w. Nichols, michael f. O'Rourke; with a contribution from craig hartley*. Arnold; Oxford University Press.
- Nichols, W. W., O'Rourke, M. F., Avolio, A. P., Yaginuma, T., Murgo, J. P., Pepine, C. J., & Conti, C. R. (1985). Effects of age on ventricular-vascular coupling. *American Journal of Cardiology*, **55**(9), 1179–1184.
- Noordergraaf, A., Verdouw, P. D., & Boom, H. B. K. (1963). The use of an analog computer in a circulation model. *Progress in Cardiovascular Diseases*, **5**(5), 419–439.
- Nowrozani, F. R., & Zareian, B. (2011). A microscopic study of the external carotid artery transitional zone of the adult male dog. *Journal of Applied Animal Research*, **39**(4), 406–411.
- O'Rourke, M. F. (1967). Pressure and flow waves in systemic arteries and the anatomical design of the arterial system. *Journal of Applied Physiology*, **23**(2), 139–149.
- O'Rourke, M. F. (1982). *Arterial function in health and disease*. Churchill Livingstone.
- O'Rourke, M. F. (1984). Wave reflections and the arterial pulse. *Archives of Internal Medicine*, **144**(2), 366.
- O'Rourke, M. F., & Avolio, A. P. (1980). Pulsatile flow and pressure in human systemic arteries. Studies in man and in a multibranch model of the human systemic arterial tree. *Circulation Research*, **46**(3), 363–372.
- O'Rourke, M. F., & Hashimoto, J. (2007). Mechanical factors in arterial aging: A clinical perspective. *Journal of the American College of Cardiology*, **50**(1), 1–13.
- O'Rourke, M. F., & Kelly, R. P. (1993). Wave reflection in the systemic circulation and its implications in ventricular function. *Journal of Hypertension*, **11**(4), 327–337.
- O'Rourke, M. F., & Nichols, W. W. (2005). Aortic diameter, aortic stiffness, and wave reflection increase with age and isolated systolic hypertension. *Hypertension*, **45**(4), 652–658.
- O'Rourke, M. F., & Taylor, M. G. (1967). Input impedance of the systemic circulation. *Circulation Research*, **20**(4), 365–380.
- O'Rourke, M. F., & Yaginuma, T. (1984). Wave reflections and the arterial pulse. *Archives of Internal Medicine*, **144**(2), 366–371.
- Olufsen, M. S. (1999). Structured tree outflow condition for blood flow in larger systemic arteries. *American Journal of Physiology Heart and Circulatory Physiology*, **276**(1), H257–H268.
- Papageorgiou, G. L., Jones, B. N., Redding, V. J., & Hudson, N. (1990). The area ratio of normal arterial junctions and its implications in pulse wave reflections. *Cardiovascular Research*, **24**(6), 478–484.

- Papageorgiou, G. L., & Jones, N. B. (1987). Arterial system configuration and wave reflection. *Journal of Biomedical Engineering*, **9**(4), 299–301.
- Parker, K. H. (2009). An introduction to wave intensity analysis. *Medical & Biological Engineering & Computing*, **47**(2), 175.
- Petersen, S. E., Wiesmann, F., Hudsmith, L. E., Robson, M. D., Francis, J. M., Selvanayagam, J. B., Neubauer, S., & Channon, K. M. (2006). Functional and structural vascular remodeling in elite rowers assessed by cardiovascular magnetic resonance. *Journal of the American College of Cardiology*, **48**(4), 790–797.
- Phan, T. S., Li, J. K. J., Segers, P., & Chirinos, J. A. (2016). Misinterpretation of the determinants of elevated forward wave amplitude inflates the role of the proximal aorta. *Journal of the American Heart Association*, **5**(2), e003069.
- Pomella, N., Wilhelm, E. N., Kolyva, C., Gonzalez-Alonso, J., Rakobowchuk, M., & Khir, A. W. (2017). Common carotid artery diameter, blood flow velocity and wave intensity responses at rest and during exercise in young healthy humans: A reproducibility study. *Ultrasound in Medicine & Biology*, **43**(5), 943–957.
- Rakobowchuk, M., Stuckey, M. I., Millar, P. J., Gurr, L., & Macdonald, M. J. (2009). Effect of acute sprint interval exercise on central and peripheral artery distensibility in young healthy males. *European Journal of Applied Physiology*, **105**(5), 787–795.
- Rakobowchuk, M., Tanguay, S., Burgomaster, K. A., Howarth, K. R., Gibala, M. J., & MacDonald, M. J. (2008). Sprint interval and traditional endurance training induce similar improvements in peripheral arterial stiffness and flow-mediated dilation in healthy humans. *American Journal of Physiology Regulatory, Integrative and Comparative Physiology*, **295**(1), R236–R242.
- Rangankar, V. P., Taori, K. B., Mundhada, R. G., & Rewatkar, A. D. (2016). Accuracy of common femoral artery doppler waveform analysis in predicting haemodynamically significant aortoiliac lesions. *Journal of Clinical and Diagnostic Research : JCDR*, **10**, TC26–TC28.
- Redheuil, A., Yu, W.-C., Wu, C. O., Mousseaux, E., de Cesare, A., Yan, R., Kachenoura, N., Bluemke, D., & Lima, J. A. C. (2010). Reduced ascending aortic strain and distensibility: Earliest manifestations of vascular aging in humans. *Hypertension*, **55**(2), 319–326.
- Rees, P. M. (1968). Electron microscopical observations on the architecture of the carotid arterial walls, with special reference to the sinus portion. *Journal of Anatomy*, **103**, 35–47.
- Reymond, P., Merenda, F., Perren, F., Rüfenacht, D., & Stergiopoulos, N. (2009). Validation of a one-dimensional model of the systemic arterial tree. *American Journal of Physiology Heart and Circulatory Physiology*, **297**(1), H208–H222.
- Reymond, P., Westerhof, N., & Stergiopoulos, N. (2012). Systolic hypertension mechanisms: Effect of global and local proximal aorta stiffening on pulse pressure. *Annals of Biomedical Engineering*, **40**(3), 742–749.
- Rider, O. J., Holloway, C. J., Emmanuel, Y., Bloch, E., Clarke, K., & Neubauer, S. (2012). Increasing plasma free fatty acids in healthy subjects induces aortic distensibility changes seen in obesity. *Circ Cardiovasc Imaging*, **5**(3), 367–375.
- Rittenhouse, E. A., Maxiner, W., Burr, J. W., & Barnes, R. W. (1976). Directional arterial flow velocity: A sensitive index of changes in peripheral vascular resistance. *Surgery*, **79**, 350–355.
- Robinson, S. C., & Brucer, M. (1939). Range of normal blood pressure: A statistical and clinical study of 11,383 persons. *Archives of Internal Medicine*, **64**(3), 409–444.
- Rogers, W. J., Hu, Y.-L., Coast, D., Vido, D. A., Kramer, C. M., Pyritz, R. E., & Reichek, N. (2001). Age-associated changes in regional aortic pulse wave velocity. *Journal of the American College of Cardiology*, **38**(4), 1123–1129.
- Sabatier, M. J., Stoner, L., Reifemberger, M., & McCully, K. (2006). Doppler ultrasound assessment of posterior tibial artery size in humans. *Journal of Clinical Ultrasound*, **34**(5), 223–230.
- Salzer, D. A., Medeiros, P. J., Craen, R., & Shoemaker, J. K. (2008). Neurogenic-nitric oxide interactions affecting brachial artery mechanics in humans: Roles of vessel distensibility vs. Diameter. *American Journal of Physiology Regulatory, Integrative and Comparative Physiology*, **295**(4), R1181–R1187.
- Segers, P., & Verdonck, P. (2000). Role of tapering in aortic wave reflection: Hydraulic and mathematical model study. *Journal of Biomechanics*, **33**(3), 299–306.
- Sherwin, S. J., Franke, V., Peiró, J., & Parker, K. (2003). One-dimensional modelling of a vascular network in space-time variables. *Journal of Engineering Mathematics*, **47**(3/4), 217–250.
- Sluyter, J. D., Hughes, A. D., Camargo, C. A., Thom, S. A. M., Parker, K. H., Hametner, B., Wassertheurer, S., & Scragg, R. (2019). Identification of distinct arterial waveform clusters and a longitudinal evaluation of their clinical usefulness. *Hypertension*, **74**(4), 921–928.
- Stergiopoulos, N., Meister, J. J., & Westerhof, N. (1994). Simple and accurate way for estimating total and segmental arterial compliance: The pulse pressure method. *Annals of Biomedical Engineering*, **22**(4), 392–397.
- Stergiopoulos, N., Young, D. F., & Rogge, T. R. (1992). Computer simulation of arterial flow with applications to arterial and aortic stenoses. *Journal of Biomechanics*, **25**(12), 1477–1488.
- Streeter, V. L., Keitzer, W. F., & Bohr, D. F. (1963). Pulsatile pressure and flow through distensible vessels. *Circulation Research*, **13**(1), 3–20.
- Suwa, N., Niwa, T., Fukasawa, H., & Sasaki, Y. (1963). Estimation of intravascular blood pressure gradient by mathematical analysis of arterial casts. *The Tohoku Journal of Experimental Medicine*, **79**(2), 168–198.
- Tomiyama, H., Komatsu, S., Shiina, K., Matsumoto, C., Kimura, K., Fujii, M., Takahashi, L., Chikamori, T., & Yamashina, A. (2018). Effect of wave reflection and arterial stiffness on the risk of development of hypertension in Japanese men. *Journal of the American Heart Association*, **7**(10), e008175.

- van den Berkmortel, F., Wollersheim, H., van Langen, H., & Thien, T. (1998). Dynamic vessel wall properties and their reproducibility in subjects with increased cardiovascular risk. *Journal of Human Hypertension*, **12**(6), 345–350.
- van den Bos, G. C., Westerhof, N., & Randall, O. S. (1982). Pulse wave reflection: Can it explain the differences between systemic and pulmonary pressure and flow waves? A study in dogs. *Circulation Research*, **51**(4), 479–485.
- Vennin, S., Li, Y., Mariscal Harana, J., Charlton, P., Fok, H., Gu, H., Chowienczyk, P., & Alastruey, J. (2021). Novel pressure wave separation analysis for cardiovascular function assessment highlights major role of aortic root. *Ieee Transactions on Bio-Medical Engineering*, **69**(5), 1707–1716.
- Westerhof, B. E., van den Wijngaard, J. P., Murgo, J. P., & Westerhof, N. (2008). Location of a reflection site is elusive: Consequences for the calculation of aortic pulse wave velocity. *Hypertension*, **52**(3), 478–483.
- Westerhof, B. E., & Westerhof, N. (2018). Uniform tube models with single reflection site do not explain aortic wave travel and pressure wave shape. *Physiological Measurement*, **39**(12), 124006.
- Westerhof, N., Bosman, F., De Vries, C. J., & Noordergraaf, A. (1969). Analog studies of the human systemic arterial tree. *Journal of Biomechanics*, **2**(2), 121–143.
- Westerhof, N., Sipkema, P., van den Bos, G. C., & Elzinga, G. (1972). Forward and backward waves in the arterial system. *Cardiovascular Research*, **6**(6), 648–656.
- Yoo, B.-S., Lee, S.-H., Ko, J.-Y., Lee, B.-K., Kim, S.-N., Lee, M.-O., Hwang, S.-O., Choe, K.-H., & Yoon, J. (2003). Procedural outcomes of repeated transradial coronary procedure. *Catheterization and Cardiovascular Interventions*, **58**(3), 301–304.
- Yoo, B.-S., Yoon, J., Ko, J.-Y., Kim, J.-Y., Lee, S.-H., Hwang, S.-O., & Choe, K.-H. (2005). Anatomical consideration of the radial artery for transradial coronary procedures: Arterial diameter, branching anomaly and vessel tortuosity. *International Journal of Cardiology*, **101**(3), 421–427.
- Zhou, Z., Xing, A.-J., Zhang, J.-N., Xia, W.-H., Su, C., Xu, S.-Y., Zhang, X.-Y., Chen, S.-H., Huang, Z., Qian, X.-X., Wu, S.-L., & Tao, J. (2021). Hypertension, arterial stiffness, and clinical outcomes: A cohort study of chinese community-based population. *Hypertension*, **78**, 333–341.

## Additional information

### Data availability statement

The raw data from the YoungAdult model will be made available upon reasonable request.

### Competing interests

The authors declare no competing interests.

### Author contributions

A.K. and J.P.M. contributed to the conception and design of the work. A.K., H.A.H., J.J.S., M.M.H.C. and J.P.M. contributed to the acquisition, analysis or interpretation of data for the work and to drafting and revising the manuscript. All authors approved the final version of the manuscript and agree to be accountable for all aspects of the work in ensuring that questions related to the accuracy or integrity of any part of the work are appropriately investigated and resolved. All persons designated as authors qualify for authorship, and all those who qualify for authorship are listed.

### Funding

J.P.M. was supported by a co-funded Career Development Fellowship from the National Health and Medical Research Council of Australia (APP1143510) and Future Leader Fellowship from the National Heart Foundation of Australia (101199). The Heart Research group at the Murdoch Children's Research Institute is supported by the Victorian Government's Operational Infrastructure Program, RCH 1000 and Big W.

### Acknowledgements

Open access publishing facilitated by The University of Melbourne, as part of the Wiley – The University of Melbourne agreement via the Council of Australian University Librarians.

### Keywords

arterial haemodynamics, cardiovascular modelling, wave reflection

### Supporting information

Additional supporting information can be found online in the Supporting Information section at the end of the HTML view of the article. Supporting information files available:

#### Statistical Summary Document

Parameters and connectivity of 1D segments

Resistance and compliance of systemic vascular beds

Raw data of average in vivo velocity and pressure waveforms

Peer Review History